

# **FIELD TRIP TO THE NORTHERN ALISITOS ARC SEGMENT: ANCESTRAL AGUA BLANCA FAULT REGION**

**By**

**Paul H. Wetmore**

Dept. of Geosciences, U. of Arizona, Tucson, AZ 85721

**Helge Alsleben**

**Scott Paterson**

Dept. of Geosciences, U. of Southern California, Los Angeles, CA 90089

**Mihai Ducea**

**George Gehrels**

**Victor Valencia**

Dept. of Geosciences, U. of Arizona, Tucson, AZ 85721

Field Trip Guide for the  
**VII International Meeting of the Peninsular  
Geological Society**

April 3<sup>rd</sup> through 6<sup>th</sup>, 2005 in Ensenada, Baja California, Mexico

## Introduction

The western continental margin of North America was characterized by a substantial component of tectonic accretion during the late Paleozoic and throughout the Mesozoic. The new continental growth that resulted from this general process is necessarily complicated. This complication arises, not only from post-accretion tectonic disruption (e.g., Suppe, 1970; Hall, 1991; Barth et al., 2003), but also from fundamental differences in the amount and type of material impinging upon, and ultimately becoming attached to, the continental margin along the strike of the paleotrench. Examples of added tectonic elements include slices of oceanic crust (e.g., Coast Ranges Ophiolite), island arcs (e.g., Seven Devils Terrane), and the sediments/volcanics deposited on the ocean floor at varying distances from spreading centers, ocean islands, and continents (e.g., Western Metamorphic Belt of the Sierra Nevada foothills). Faults, of variable type, must have existed between each of these tectonic elements to have accommodated the differential displacements between each element and ultimately serving to join them to each other. These combining structures can have deformational histories associated with them that are comparable in scale and magnitude to the structures that juxtapose accreted elements with the continental margin but, are often less-well defined geologically.

The Peninsular Ranges batholith is a world class example of a laterally-zoned batholith, with a mafic western (outboard) zone and a felsic eastern zone. Several data sets document the existence of east-west transitions between eastern, central, and western batholith-parallel zones (Fig. 1). These data include rare earth elemental (REE) abundances (Gromet and Silver, 1987); oxygen isotopic signatures (Taylor and Silver, 1978); and Sr initial ratios and  $\epsilon_{Nd}$  determinations from plutonic rocks (DePaolo, 1981). In addition, the Fe-Ti oxide mineralogy of the batholith exhibits an east-west transition where plutons of the western zone contain magnetite and ilmenite while those of the eastern zone contain only the latter mineral phase (Gastil et al., 1990).

The above plutons intrude four major lithostratigraphic belts which parallel the long axis of the batholith (Gastil, 1993). These are, from east to west, Late Precambrian to Permian miogeoclinal strata, Ordovician to Permian (Early Triassic?) slope basin deposits, (Late?) Triassic to Cretaceous "back-arc" sedimentary rocks, and Jurassic(?) to Cretaceous arc volcanics. The Peninsular Ranges is subdivided into three zones (eastern, central, and western), the trends of which parallel the batholith (Fig. 1). Typically the eastern zone includes miogeoclinal and slope basin deposits, the central zone "back-arc" sedimentary rocks, locally overlying slope basin strata, and the western zone volcanic rocks (Gastil, 1993).

These across-strike variations of the host rock stratigraphy and intrusive rocks have been interpreted to reflect a change in basement composition (e.g., DePaolo, 1981; Silver and Chappell, 1988), where the primitive western zone, with its island arc signature, is underlain by oceanic lithosphere, and the eastern zone is underlain by older lithosphere of continental composition. These observations and interpretations have provided the foundations for a series of tectonic models seeking to explain the juxtaposition of these disparate lithospheric types.

The original modern regional syntheses of Peninsular Ranges geology were completed by Gordon Gastil and coworkers (Gastil et al., 1975; 1981). In these studies Gastil et al. not only identified many of the across strike variations to the PRb, but also several north to south transitions to the geology/geophysics of the volcanics-dominated

western Peninsular Ranges. These differences appeared to be most pronounced across the trace of the ABF. They include a change in the environment of deposition of the volcanic and associated sedimentary strata, an apparent age break, and dramatic steps in the gravity and aeromagnetic signatures across the fault. Specifically, the Santiago Peak arc segment to the north of the ABF is characterized by subaerially deposited Jurassic to Early Cretaceous volcanics (although later constrained to just Early Cretaceous; Wetmore et al., 2003a) and both low gravity and magnetic signatures. In contrast, the subaqueously deposited Early Cretaceous (Aptian-Albian) volcanics/volcaniclastics of the Alisitos arc segment to the south of the fault exhibits both a gravity and magnetic high. In the accompanying tectonic model, Gastil et al. (1981) proposed that the western zone north and south of the fault were once a continuous fringing arc rifted from the continental margin and subsequently and diachronously reaccreted. They argued that the Santiago Peak arc segment was reaccreted first in the Aptian-Albian and the Alisitos arc segment late in the Albian.

Wetmore et al. (2002; 2003a) revisited the concept of a potential Mesozoic history to the ABF approximately 20 years later. They identified several additional variations in the geology of the two western arc segments, all seemingly centered on the newly identified aABF, a southwest vergent ductile shear zone located approximately 2-3 km south of the active ABF (Fig. 2 and 3a). These additional variations include the presence or absence of Late Triassic-Jurassic continentally-derived turbidite strata, the structural relationships between Cretaceous volcanics and continentally-derived strata, the presence or absence of xenocrystic Precambrian zircons in Cretaceous volcanics/plutonics, and the amount and location of deformation exhibited by the Cretaceous strata.

Their interpretation of these and the previously identified variations in geology across the aABF resulted in a different tectonic model than that proposed by Gastil et al. (1981). Wetmore et al. (2003a) argue that the Late Triassic-Jurassic turbidite sequences, named the Bedford Canyon Complex, present to the north of the ABF exhibit a geometry and style of deformation (Sutherland et al., 2002) consistent with that commonly observed within upper levels of an accretionary prism (e.g., Sample and Moore, 1987). The presence of Precambrian detrital zircons (Gastil and Girty, 1993) and olistostromes with detrital zircon signatures equivalent to parts of the southern North American Paleozoic passive margin sequences (Gehrels et al., 2002) further suggest that this accretionary prism formed in situ along the southwestern margin of North America. The Early Cretaceous Santiago Peak Volcanics are likewise interpreted to have been emplaced in their present position atop the Bedford Canyon Complex. This follows from the lack of observed shear across exposures of the contact between the two groups of strata (Herzig, 1991; Sutherland et al., 2002), the presence of Precambrian xenocrystic zircons in both plutonics and volcanics of the Santiago Peak arc (ages consistent with those observed in the underlying Bedford Canyon Complex; Anderson, 1991; Herzig, 1991; Carrasco et al., 1995; Premo et al., 1998), and dikes that cut the underlying Bedford Canyon Complex, the contact, and can be shown to have fed flows in the overlying Santiago Peak Volcanics (Herzig, 1991). Hence, Wetmore et al. (2002; 2003a) argue that the Santiago Peak arc was a continental margin arc built on and through the earlier formed North American accretionary prism.

In contrast to the Santiago Peak arc segment, the Alisitos arc segment to the south of the aABF is interpreted to have been an exotic island arc that developed on and through

oceanic lithosphere not associated with the North American margin prior to its accretion in the late Early Cretaceous (Johnson et al., 1999a). This follows from the observations that the volcanic and plutonic rocks of the arc segment have not yielded Precambrian zircons (Carrasco et al., 1995; Johnson et al., 1999a, b, 2003; Tate et al., 1999), as well as the presence of a broad (15->30 km) fold and thrust belt that is developed within the Cretaceous volcanoclastic strata (Alisitos Formation) along the boundaries of the arc segment with continental margin sequences, including the Santiago Peak Volcanics and Bedford Canyon Complex to the north (Johnson et al., 1999a; Schmidt, 2000; Wetmore et al., 2002).

In summary, we argue that the western zone of the PRb did not form as a single tectonic entity but rather the arc segments north and south of the aABF came to be juxtaposed with the North American continental margin at different times and through different tectonic scenarios. The basement to the Santiago Peak arc, a continental margin arc, developed on and through the Late Triassic through Jurassic North American accretionary prism. The Alisitos arc developed on oceanic crust during the Early Cretaceous and was combined with the continent across large west and southwest-vergent ductile shear zones (e.g. Main Mártir Thrust). The aABF is the ductile shear zone that juxtaposes the two arc segments and the geology associated with this structure will be the primary focus of this field trip.

### **Field Trip Overview and Regional Geology of the Northern Alisitos Arc**

Before describing the geology of the focus area of this field trip it is important to note that much of the text herein derives from several previous publications. Specifically, introductory material and descriptions of the structures, geochronology, and geochemistry of the northern Alisitos arc are lifted from Wetmore et al. (2003a) and two manuscripts, one specific to the deformation associated with the aABF submitted to Tectonics (Wetmore et al., in review) and the other focused on the petrology and geochemistry of the various plutonic rocks of the aABF region (in preparation).

#### **The Agua Blanca faults: active and ancestral**

The geology of the region described below is strongly defined by the evolution of the active and ancestral Agua Blanca faults. The active ABF is a dextral strike slip fault that transfers slip out of the Gulf of California and into the Continental Borderlands (Allen et al., 1960, Suarez-Vidal, 1991; Rockwell et al., 1993; Legg et al., 1991). The active fault can be traced ~130 km from the Main Gulf Escarpment near San Matias Pass to Punta Banda (Fig. 1). The fault is generally a very distinct zone, less than 0.5 km wide in Valle Agua Blanca, but diverges into northern and southern branches near the southern end of Valle Santo Tomás. Mapping in Valle Agua Blanca by Allen et al. (1960) shows a Cretaceous quartz diorite intrusion cut by the ABF appears to be offset ~22 km, which is inferred to be the maximum displacement on the active fault.

In the original geologic synthesis by Gastil et al. (1975, 1981), the ABF is identified as an inherited Cretaceous structure that initially formed as a sinistral transform fault accommodating the diachronous accretion of the Santiago Peak and Alisitos arc segments. This designation was made to explain north to south differences between the two arc segments without specific knowledge of the geology in the area around the ABF. The ancestral Agua Blanca fault (aABF) is a separate structure from the active fault that

is characterized by a late Early Cretaceous dip slip (thrust) history. Details concerning the aABF are discussed below (Fig. 2 and 3).

### **Stratigraphy and Provenance of the Alisitos Formation**

The Early Cretaceous depositional history of the Alisitos arc segment is represented by the Alisitos Formation. The stratigraphy represented in Figure 4 includes 6 km of section contained within three fault-bound blocks (note that the aABF truncates the top of the section and the San Vicente pluton intrudes the bottom of the section). This section was constructed based on detailed observations made through two parallel transects from the aABF to the northern margin of the San Vicente pluton. One transect was completed along Cañon Agua Caliente. The other transect was completed through the unnamed cañon immediately north of Cañon El Trigo, through Canada Suazalita, and into several small unnamed valleys north of the Balbuena pluton. It is important to note that the stratigraphy of an arc system like that represented by the Alisitos Formation is characterized by dramatic along strike variations (Fackler-Adams and Busby, 1998). Therefore, the stratigraphy presented here is very site specific. It should also be noted that the Alisitos Formation throughout this study area is metamorphosed to at least lower greenschist grade. Descriptions of the stratigraphy presented here, however, are given in terms of protolith.

The structurally lowest block in the column includes ~1,600 m of section. The base of this block includes a thick (>50 m) unit composed of silicic ashes. This unit is distinctive in that it is one of the thickest individual volcanic units observed anywhere in the study area and that it is characterized by well-developed columnar jointing. Overlying this unit is a thick (~1000 m) succession of alternating thin (<1m) volcanic ash fall tuffs and similarly scaled argillites with rare sub-meter-scale limestones. Accretionary lapilli are observed within at least two of the ash fall tuffs, one of which is within a couple of meters, stratigraphically, of a limestone unit. Near the top of the lowest fault-bound block below the El Ranchito fault and above a small unnamed fault are two coarse grained volcanoclastic sandstones bounding a relatively thick (50-100 m) limestone unit which is strongly recrystallized in this study. In satellite images, this limestone unit can be traced discontinuously from the coast at Punta China to the northern Sierra San Pedro Mártir (Fig. 2). As such this is the most regionally extensive unit for the entire western zone of the Peninsular Ranges (Silver et al., 1963). Similar limestones are also reported from the San Fernando area (Beggs, 1984).

The middle fault-bound section of the stratigraphic column shown in Figure 4 includes approximately 2000 m of section. The bottom two thirds of the section is dominated by alternating sequences of primary volcanic rocks and redeposited volcanoclastic sandstones. The primary volcanic rocks are typically plagioclase-feric, lithic-rich ash fall or flow tuffs that range between 2 and 10 m in thickness and commonly uphold many of the strike ridges in the area. In addition to the tuffs are at least two basaltic lava flows that reach thickness of 10 m and exhibit abundant pillows in most exposures. Volcanoclastic sandstones are typically thin (<1 m) and very coarse grained with grading toward upper medium grained at the tops of individual beds commonly observed. Grains are typically angular to subrounded and exhibit numerous post-depositional fractures. A single, moderately thick (2-5 m) limestone (marble) unit is also present near the middle of this volcanics and sandstones-dominated part the middle

section of the column. Unlike the recrystallized limestones of the lower section, this unit contains abundant centimeter scale volcanic and sandstone clasts that increase in concentration near the bedding surfaces of the unit. This seems to suggest that they were incorporated during shearing.

The upper third (>400 m) of the middle fault-bound section (Fig. 4) is quite different than the majority of this part of the column due to the presence of a thick succession of argillites. This succession of argillites is generally homogeneous with the exception of a few thin (<0.5 m) coarse grained sandstones.

The uppermost fault-bound block of the stratigraphic column (Fig. 4) includes ~2200 m of section and is considerably more variable in composition than that of the two lower blocks. The lower half of the upper-most part of the section includes a heterogeneous mix of primary volcanic rocks intercalated with lesser volcanoclastic sandstones and argillites, as well as rare limestones (marbles). The volcanic rocks are, themselves, a heterogeneous mix of lava flows, and ash falls and flows with a broad range in compositions from basalts to dacites/rhyolites(?). A single thick (>10 m) basalt flow located near the middle of this part of the section possesses abundant pillows. However, an ash fall tuff possessing accretionary lapilli was observed less than a kilometer away and only ~500 m further up section. Limestones (marbles) present in this part of the column are typically thin ( $\leq 1$  m), discontinuous, and disseminated pods. The relative abundance of various rock types changes markedly between the bottom half and top half of the uppermost section of the column. In the top half, while primary volcanic rocks (ash fall/flow tuffs) do occasionally interrupt the section, the dominant rock type is argillite. A couple of very thin (~0.5 m) and discontinuous limestones (marbles) were observed in this part of the section but due to their discontinuous character and high strains in the region it was not clear that they were in section as depositional unit or were dislodged blocks (olistostromes?).

The faults and ductile strain affecting the strata of the study area introduce substantial uncertainty into the stratigraphic reconstruction shown in Figure 4. Given the lack of temporal control on individual units within the column it is impossible to know the degree to which the El Ranchito and El Tigre faults have duplicated the section. The total throw on any of the faults in the study area is difficult to assess due to the lack of distinctive stratigraphic marker units. However, the repetition of general stratigraphic trends indicates the possibility that all three fault bound blocks are lateral equivalents. Specifically, each block is characterized by a primary volcanic rock dominated base that grades upward into increasingly sedimentary strata dominated upper parts. Such short wavelength repetition of the section is also permissible given the lack of a metamorphic step across either the El Ranchito or El Tigre faults. The large magnitude and lithology-dependent variability of ductile strains throughout the study area further complicate the accuracy of the reconstructed stratigraphic column as strain data indicate that unit thicknesses have been substantially modified during regional contraction. Conservative estimates of shortening are ~50% (e.g. Fig. 3d, 3e, and 4) in a direction approximately normal to bedding planes throughout the region indicating initial unit thicknesses may have been nearly double. However, it should be noted that nearly all strain measurements were completed on lithic rich volcanoclastic rocks that typically exhibit strain intensities intermediate between lava flows and argillites (e.g. Paterson et al., 1995). Evidence for lithologically controlled variation in strain was observed throughout this field area.

U-Pb analysis of detrital zircon populations was conducted on two samples of coarse-grained sandstone collected from the top of the lower-most section (sample 6/6/00-F), and from ~800 m below the top of the middle section (sample 5/19/00-A; Figs. 4 and 5). Twenty-two and fifty-three zircons, respectively, were analyzed by George Gehrels using a Laser Ablation Multi-Channel Inductively Coupled Plasma Mass Spectrometer (LA-MC-ICPMS) at the University of Arizona. The  $^{206}\text{Pb}/^{238}\text{U}$  ages for the zircons analyzed range from  $102.9 \pm 3.3$  to  $1550.1 \pm 61.7$  Ma for sample 6/6/00-F and from  $100 \pm 2.8$  to  $2758 \pm 16.9$  Ma for sample 5/19/00-A (Fig. 6). Nearly all of the zircons analyzed from sample 6/6/00-F (20/22) yield latest Late Jurassic through latest Early Cretaceous ages and exhibit an almost continuous range in ages from ~145 Ma to 115 Ma where the next youngest or oldest ages in not much more than ~2 m.y. difference. However, a >10 m.y. gap exists between the youngest zircon age at 102.9 Ma. Also, two early Middle Proterozoic ages were also determined for zircons from this sample. Conversely, less than half of the zircons from sample 5/19/00-A yield Mesozoic ages with a much greater percentage (~40%) of Paleozoic and Precambrian ages, including two that yield Archean ages. Two weak clusters are represented by five grains yielding Early Cretaceous ages with one at ~110 Ma (defined by three grains) and another at ~120 Ma. Similar to the former sample, ages from sample 5/19/00-A exhibit a continuous range from 131 Ma to 152 Ma where typically less than a few million years separates any two consecutive ages. Clusters of ages greater than ~152 Ma are typically defined by only two grains until ~1430 Ma where five (5) earliest Middle Proterozoic ages form a distinct cluster and again at ~1730 Ma, where five (5) more grains form another cluster of latest Early Proterozoic ages.

When these results are combined with observations of the Alisitos Formation stratigraphy from elsewhere in this arc segment (Allison, 1955, 1974; Beggs, 1984; Suarez-Vidal, 1986; Fackler-Adams, 1997; Johnson et al., 1999a; Robert Douglas, personal communication, 2003; Alsleben, unpublished mapping) a consistent general depositional architectural picture emerges. Suarez-Vidal (1986) was one of the first to note that northeastern and eastern exposures of the Alisitos Formation are characterized by relatively deep water deposits with lesser amounts of primary volcanic rocks (e.g. lava flows and ash fall/flow deposits that have not been remobilized). Subsequently, Johnson et al. (1999a) note that in the Sierra San Pedro Mártir region (Fig. 1) the Alisitos Formation can be subdivided into a western volcanics-dominated belt and an eastern volcanoclastic and sedimentary rock-dominated belt. Scott Johnson (personal communication, 2002) also reports an overall grain size reduction toward the east and structural top of the section in the northern Sierra San Pedro Mártir. Robert Douglas (personal communication, 2003) similarly reports observing deep water deposits overlying shallow water reef limestones in the carbonate quarry at Punta China near the type section for the Alisitos Formation. The potential structural duplication, notwithstanding, the transition from coarse sandstones and lithic rich volcanoclastic rocks to relatively fine grained argillites in the middle and upper blocks of the section represented in Figure 4 also seems to indicate a late phase of subsidence in the aABF region.

The above discussion appears to confirm that a basin did exist along the northern and eastern sides of the Alisitos arc and that this basin likely experienced a subsidence event. Scenarios proposed to describe the tectonic setting of this basin are few in number and

typically quite simple. Cathy-Busby and coworkers (Busby et al., 1998; Fackler-Adams and Busby, 1998) view the Early Cretaceous Alisitos arc as a rifted fringing arc and as such describe this basin as a back arc basin. Alternatively, Johnson et al. (1999a) viewed these deposits as forming behind the Alisitos arc in an interarc or remnant ocean basin that formed as this west-facing arc approached the continental margin.

The general description of the basin appears to be very compatible with a back-arc setting. That is, a rapidly subsiding basin built upon the arc volcanics. However, two key relationships appear to be inconsistent with this model. First, detrital zircons from higher in the section contain a much greater proportion of grains yielding Precambrian and Paleozoic ages than samples from lower in the section. This suggests that the source of these zircons, the continental margin, was growing more proximal during the evolution of this basin. Secondly, initial deposition in this basin occurred between 110 and 115 Ma as indicated by the detrital zircon data from this study and the 115 Ma age given by Johnson et al. (2003), which was at most ~7 m.y. prior to the final close of the basin at ~108 Ma as indicated by the youngest plutons which intrude the deformed sediments of this basin (i.e., the Balbuena pluton (this study) and the San Jose pluton, Johnson et al., 1999a and 2003). This seems to limit the possibility that this was a rifted back-arc basin (e.g. Lau Basin, Marsaglia, 1995) since they tend to form due to the subduction of relatively old oceanic lithosphere (>80 Ma) causing trench retreat (e.g., Molnar and Atwater, 1978). Thus, the transition from extension to contraction would require several million years, likely >20 m.y., in order for the age of the subducting lithosphere to decrease sufficiently to change the stress regime.

A potential alternative to the rifted back arc basin model is exemplified by the collisional foredeep of western Taiwan. There the Asian continental margin is presently being subducted beneath the Luzon arc along the western side of the Philippine Sea Plate (Lundberg et al., 1997). Due to the buoyancy of the subducting Chinese passive margin the down-going slab has developed numerous normal faults related to the flexural deformation (Chou and Yu, 2002). As a result, slow subsidence associated with late passive margin evolution has locally been overprinted by rapid subsidence associated with the flexural depression and normal faulting. Sediment provenance has also switched from western continentally-derived sources to the increasingly proximal arc to the east. Ultimately these sediments, and the basin in which they are being deposited, will be incorporated into the fold and thrust belt of the western Foothills of Taiwan. Similarly, we believe that it is possible that as the Alisitos arc approached the North American margin and its trench, the eastern or back side of the Alisitos arc was rapidly depressed and a new and ever proximal sediment source in the continent to the east became increasingly prevalent in the basin deposits. Subsidence rates in this case may be comparable to those observed in typical extensional basins.

### **Structural Geology: northern Alisitos arc segment**

A relatively detailed (1:5,000 scale) map was completed along a corridor through the northern Alisitos arc from the town of San Vicente northeast to the aABF (Fig. 2 and 3). This particular section was chosen due to the relatively complete section through the Alisitos Formation that was not everywhere affected by the emplacement of intrusive bodies. In general, the mapped region is a brittle-ductile fold and thrust belt with several brittle-ductile, dip-slip shear zones, multiple groups of subhorizontal folds of varying



tightness and inclination, and numerous intrusive bodies with temporal and spatial relationships that vary with respect to the regional deformation. The following section will include some detailed discussion of a variety of structural aspects of the aABF region including faults and folds, lineations and kinematics, strain, and intrusive bodies.

*Faults and Folds:* A number of discreet faults and minor shear zones were observed between the town of San Vicente and the aABF. The most important among these faults are, from northeast to southwest, the aABF, the El Tigre fault, and the El Ranchito fault. The aABF is a mylonite shear zone, oriented N72°W 72° NE, and located between two and three kilometers southwest of the active ABF along the south side of the Valle Agua Blanca. Good exposure of the structure is limited to two locations in the study area, immediately northwest of the Arce pluton ( $K_A$ ), which truncates the shear zone, and another approximately five kilometers further northwest near the western limit to Valle Agua Blanca (Figs. 2 and 3). The shear zone is nearly 100 m wide in the former exposure and at least 50 m wide in the latter. A third exposure of lesser quality is also present southeast of the Arce pluton but is strongly overprinted by the intrusion.

Two well developed foliations are preserved in the shear zone, the older foliation, which is continuous, parallels the strike and dip of the zone and the younger, a spaced crenulation foliation, overprints the former foliation and is oriented N46W dipping 65° NE (Fig. 7b). Locally, the primary foliation is folded (cm-scale) and the crenulation foliation is axial planar to these folds (Fig. 7c). Strain is immeasurably large within the shear zone as all original depositional features have been obliterated.

The El Tigre fault is inferred to be present in an area approximately 2-3 km southwest of the Balbuena Pluton ( $K_{BP}$ ), due to the geometry of folds and a rapid facies transition (Fig. 3). Immediately southwest of the inferred position of the El Tigre fault is the overturned limb of a large northeast-dipping fold that is cored by argillites. To the northeast of this proposed structure is the southwest-dipping limb of an upright anticline comprised of thick successions of volcanics. While direct observation of this fault has not been made in this area, its presence is supported by observed gradients in strain intensity toward the proposed fault from the southwest (discussed below).

The El Ranchito fault is observed at several locations including along Mexican Highway 1, in Cañon El Trigo (north of R. Sandoval), and near Rancho El Ranchito (Figs. 2, 3, and 7a). In each location the fault, which dips steeply ( $>65^\circ$ ) to the northeast, structurally overlies the prominent limestone unit discussed above and a second lesser fault which is everywhere observed below the limestone. In Cañon El Trigo, where the fault is best exposed, it is characterized by a thin (~0.3 m) layer of cataclasite that is overlain by one to two meters of fault breccia. Elsewhere the fault is defined by a dramatic increase in the intensity of foliation and ~1 m thick horizons of breccia with sparse exposures containing cataclasites. The small fault below the prominent limestone unit parallels the El Ranchito fault throughout the study area but is everywhere less well defined, typically characterized by a zone of small shear fractures and thin breccia horizons with abundant epidote-chlorite mineralizations.

Folds mapped between the San Vicente and the aABF exhibit continuous changes in tightness and the dip of their axial surfaces from one fault bound block to the next (Fig. 3). However, axial traces for all folds are subparallel at  $\sim 300^\circ$  and in each area exhibit some moderate hinge thickening while lacking features that would indicate shear along

bedding contacts (e.g., slickenlines, streaking). At least two pairs of close to tight (interlimb angle between 25-50°), upright and horizontal folds are present between the northeastern margin of the San Vicente Pluton and the El Ranchito fault. The average crest to crest wavelength for these folds is approximately 1 kilometer. A single, overturned tight to isoclinal (interlimb angle <15°) fold is present between the El Ranchito and El Tigre faults (between 1 and 3 km) in the main part of the study area. The axial surface to this fold dips steeply toward the northeast at ~75°. Much of the overturned limb to this fold appears to be cut-out by the El Tigre fault. No less than five pairs of tight to isoclinal, commonly overturned folds are present between the El Tigre fault and the aABF. The axial surfaces for these folds typically dip steeply toward the northeast (~70-80°) but those closest to the El Tigre fault possess upright and even steeply southwest dipping surfaces. The average crest to crest wavelength for all of these folds is ~1 km but may decrease substantially within a few kilometers of the aABF.

*Lineations and Kinematics:* In most instances exposures of the Alisitos Formation and the Piedra Rodada pluton which exhibit subsolidus foliations also possessed a true stretching lineation (Fig. 3c). This is true even though the measured fabric ellipsoids for nearly all samples analyzed from this region were strongly oblate in shape. The lineation is commonly defined by the elongation of lithics, phenocrysts, or mafic microgranitoid enclaves in the case of the Piedra Rodada. The mean orientation for all measured lineations from the Alisitos and Piedra Rodada was 72°-037°. However, individual measurements around some structures were consistently different from the norm. In particular, while measurements from fold limbs were typically steeply plunging toward the northeast, the trends of those near hinges were commonly subparallel to the axial trace of the folds, yet were still relatively steeply plunging.

A large number of reliable kinematic indicators, nearly all indicating the same sense of shear, are present throughout the field area. These include asymmetric clasts and folds (cm-km scale) within the Alisitos Formation, and asymmetric mafic enclaves, mica-fish, and S-C fabrics in the subsolidus deformed Piedra Rodada pluton ( $K_{PR}$ ; Fig. 10a-c). Nearly all shear sense determinations from lineation parallel-foliation perpendicular sections indicate a northeast over southwest, reverse shear sense. Shear sense indicators near all three major faults (aABF, El Tigre, and El Ranchito) unambiguously suggest northeast side up-reverse shear. Only three exceptions to the northeast side up-reverse shear sense were observed in the study area; (1) within the structural aureole of some of the plutons, (2) along a small fault located just north of Rancho Sandoval (~2 km north of San Vicente), and (3) on the overturned limbs of some of the folds within ~3 km of the aABF.

The kinematic shear sense determined from the Alisitos Formation within the structural aureole of the Balbuena pluton ( $K_{BP}$ ) is markedly different from that observed in nearly every other part of the study area. In particular, along the northwest and southeast margins where bedding contacts and kilometer-scale folds exhibit dramatic deflections, lineations are often scattered and inconsistent over very short distances. Kinematic indicators in the most deflected portion of the northwestern margin yield both northwest-side-up reverse, and dextral shear. Conversely, those along southeastern margin of the Balbuena the kinematic indicators commonly indicate northwest-side-down normal and sinistral shear.

Two additional locations where kinematic indicators suggest a shear sense other than northeast-side-up reverse shear include a small fault near the margin of the San Vicente pluton ( $K_{SV}$ ) and on the alternating limbs of overturned folds south of the aABF (Fig. 3). Drag of bedding contacts along a small dip-slip fault ~200 m north of Rancho Sandoval (Fig. 10c) is consistent with normal displacement across the structure. Similarly, asymmetries to volcanic lithics and phenocrysts, and small (cm-scale) folds within strata on the overturned limbs of some of the folds present to the south of the aABF are consistent with a northeast-side-down normal sense of displacement.

Asymmetries in clast shapes and folds observed in faces oriented normal to both foliations and lineations were identified in several exposures within ~5 km of the aABF. While these examples are not nearly as well developed as those for lineation parallel sections they do exhibit a consistent sinistral shear sense. At greater distances from the aABF asymmetries in this plane are less commonly observed and do not always exhibit a consistent shear sense.

*Plutons:* Several intrusive bodies are present throughout the Alisitos portion of the study area and their apparent contribution to the structural evolution to this part of the arc is somewhat varied. The northern most body that at least partially intrudes the Alisitos arc is the Arce pluton ( $K_A$ ; Fig. 3). Fabrics within this body are largely magmatic and weak, and on average parallel the long axis of the pluton and the trends of regional structures (e.g. aABF). The Arce pluton cuts the aABF along its northwestern and southeastern margins without deflection of the shear zone or foliations therein.

Immediately south of the Arce pluton is the Piedra Rodada pluton ( $K_{PR}$ ) which is one of the few known bodies intruding the Alisitos Formation that exhibits a strong subsolidus fabric (Fig. 3b). Along the southwest side of the Piedra Rodada the foliation is typically magmatic and well defined by plagioclase, biotite, hornblende, and mafic microgranitoid enclaves. However, within ~1 km of the northeastern margin of the pluton and <1.5 km of the aABF the foliation becomes increasingly subsolidus as indicated by the formation of quartz ribbons, mica-fish with wings or tails, and fractured feldspar and hornblende phenocrysts. In both examples, magmatic and subsolidus, the fabric exhibits a very consistent orientation of  $\sim 295^\circ$   $\pm 76^\circ$ . Within approximately 200 m of the northeastern contact millimeter to centimeter-scale C-type shear bands are observed that increase in abundance and intensity toward the margin until a strong S-C fabric is observed right at the contact. This fabric appears to continue into the country rocks to the northeast of the pluton toward the aABF, as well as along strike toward the northwest past that margin of the Piedra Rodada.

The next intrusive body south is the Balbuena pluton ( $K_{BP}$ ) which is characterized by a relatively weak magmatic fabric throughout and inconsistent contact relationships with the surrounding Alisitos Formation (Fig. 3). Magmatic fabrics within the Balbuena exhibit no consistent relationship with either internal or external contacts of the pluton, or with regional fabrics and structures. However, the Balbuena is associated with a well defined structural aureole that is as much as 1.5 km wide along the northwest and southeast sides of the intrusion and less than ~0.5 km to the northeast and southwest. The structural aureoles along the northwest and southeast sides of the pluton are particularly interesting due to dramatic deflections of bedding and folds away from regional orientations. An overturned syncline whose axial surface strikes  $\sim 300^\circ$  and dips  $\sim 75^\circ$  to

the northeast at distances greater than ~1 km from the northwest margin of the Balbuena exhibits an ~70° counterclockwise rotation in strike and becomes fully upright within 0.5 km from the contact. Similarly, a series of folds along the southeast side of the Balbuena exhibit a nearly 80° clockwise rotation within 0.5 km from that contact. In other parts of the Balbuena, however, this strongly deflected structural aureole appears to have been mechanically removed by processes such as stoping. For example, in the western and northern corners of the intrusion folds and bedding are truncated discordantly at the margins without significant deflection beginning at distances greater than a few meters to 10's of meters (Fig. 3a). This late stage mechanical disintegration of the structural aureole appears to be caused by emplacement of the outmost phase of the Balbuena which forms a crescent shape around the inner two phases (Wetmore et al., 2001).

The San Vicente pluton ( $K_{SV}$ ) is a very long, almost sheet-like intrusion that is one of the larger bodies in this part of the Alisitos arc. The San Vicente pluton in this study area exhibits only weak magmatic foliations that tend to strike northwest-southeast, parallel to both the margins of the intrusion and to the trends of regional structure in the surrounding country rocks. Locally, however, the margin of the San Vicente pluton does cut obliquely across bedding without observed deflection.

Strain: In order to quantify the intensity of deformation within the study area tectonic strains were measured in 26 samples. Sample collection was focused on polymictic, lithic-rich volcanoclastics to avoid the inadvertent inclusion of measurements of pumice clasts, which tend to exhibit extreme post-depositional compactions (Wetmore and Paterson, 2002, Wetmore et al., in review). The samples used in this study were collected from a number of different localities within or near the various structures present in the map area and discussed above (Fig. 3d and 3e). These localities include the hinges and limbs of folds, structural aureoles of intrusive bodies, both hanging and footwalls of faults, and areas very distant to any of these structures/deformation. Figure 5 shows the distribution of sample localities and Table 2 includes, not only the strain data from this study, but also all such data collected from all Peninsular Ranges samples (Griffith and Hoobs, 1993; Chavez-Cabello, 1998; Johnson et al., 1999b; Schmidt, 2000).

To measure strain three mutually perpendicular, but otherwise arbitrary, cuts were made of each sample and an XYZ coordinate system was set up using the intersections of each face as axes. On each face the length of the longest and shortest (in a direction perpendicular to that of the long dimension) axes and the orientation of the long axis relative to the XYZ reference frame were measured for 30 to 100 markers (lithics). Three dimensional fabric ellipsoids were calculated from two-dimensional ellipses using the technique of Shimamoto and Ikeda (1976) or were calculated directly from the data measured from the three orthogonal cuts following Miller and Oertel (1979).

The strains measured from samples collected in the aABF area exhibit a range in intensity with the largest gradients associated with large shear zones and pluton aureoles. The intensities range from 0.08 (4.4% shortening in the z-direction) to >1.6 (>80% shortening in the z-direction) (Table 2). In general, the shapes of the strain ellipsoids exhibit a range from plane strain to oblate with only those with the smallest intensities exhibiting prolate shapes (Fig. 8).

While strain intensity does appear to exhibit an overall increase northeast toward the aABF the distribution of high strain intensity is not related solely to that structure. Figure

8 is a modified Flinn plot showing all strains calculated from this study area with those from samples collected within the structural aureoles of intrusive bodies differentiated from those collected from localities between these bodies. This plot shows that samples collected from pluton aureoles overlap with those proximal to large shear zones. Figure 9a-c illustrates the heterogeneous character of strain throughout the study area with three different strain parameters (intensity, z-direction shortening, and Lodes parameter) plotted with respect to the sample location relative to the aABF. Also shown on this figure are the approximate locations of the El Tigre and El Ranchito faults. While a gradient in strain intensity/percent shortening, increasing toward the northeast (aABF), is present from ~7 km south of the fault, a second region of elevated strain is also present in both walls of the El Ranchito fault. In contrast, the area surrounding the El Tigre fault is characterized by relatively low strain intensities. Figure 9c, a plot of Lodes parameter for each sample relative to the distance from the aABF exhibits no consistent relationship between strain ellipsoid shape and proximity to any of the major faults in the study area.

### **Geochronology and Geochemistry**

U/Pb isotopic analysis on zircon separates was completed on six plutonic samples from the San Vicente-Agua Blanca Fault area. The plutons sampled include the Santo Tomás ( $K_{ST}$ ; sample PHW 5/29/01-B) and Agua Blanca ( $K_{AB}$ ; sample PHW 1/8/03-H), both from north of the aABF, and the Piedra Rodada ( $K_{PR}$ ; sample PHW 7/6/01-S), two phases from the Balbuena pluton ( $K_{BP}$ : samples PHW 6/9/01-B and PHW 6/9/01-F), and the San Vicente pluton ( $K_{SV}$ ; sample PHW 1/12/03-A) all from south of the aABF. Between 20 and 25 zircon crystals were analyzed from each sample using an LA-MC-ICPMS at the University of Arizona. See Wetmore et al. (in review) for details on the analytical procedures and the raw data for individual spot analyses.

Analyses of 137 grains from the six plutonic samples produced one latest Jurassic age and the rest were late Early Cretaceous to early Late Cretaceous. All plutons yield late Early Cretaceous ages (Fig. 11, Table 4) which is consistent with a late syn-tectonic to post tectonic timing of emplacement inferred from contact relationships with deformed host rocks and the lack of subsolidus fabrics within most bodies. The Piedra Rodada pluton, however, with its well formed and asymmetrically distributed high temperature subsolidus fabrics along the aABF side of the intrusion, indicates that shear across that fault continued after 105.5 Ma.

An additional purpose for generating the geochronologic data for the plutons chosen was to further test the observation that Santiago Peak plutons possess at least some component of Precambrian xenocrystic zircons incorporated during the intrusion through the metasedimentary basement to that part of the arc. However, such xenocrysts were not identified in either of the two plutons sampled from north of the aABF, although the Santo Tomás pluton did include a single grain yielding a Late Jurassic age (Wetmore et al., in review). Consistently, however, no grains yielding ages older than Early Cretaceous have been analyzed from samples of Alisitos plutons.

These observations raise some questions concerning interpretations based on the importance of the presence or absence of such xenocrystic zircons in plutonics. It should be noted that the vast majority of U/Pb ages for intrusives from the Peninsular Ranges were completed by ion dissolution thermal ionization mass spectrometry on multiple

grains (e.g. Anderson, 1991; Premo et al., 1998). While all such analyses of intrusives from the Santiago Peak have resulted in the inferred presence of some component of inheritance the lack of similar observations from the LA-MC-ICPMS method may result from significant differences in the methods and not necessarily from a geologic cause. Even though analyses from this study were done in situ on the cores of zircon grains certain sample preparation procedures, such as hand picking grains to be analyzed, may have biased the sample and the resulting data away from identifying older inherited grains. Such potential biases notwithstanding, it does seem unlikely that with over 200 individual zircon grains analyzed (Johnson et al., 1999a, 2003; Wetmore et al., in review) from Alisitos arc plutonics using both SHRIMP and ICPMS methods that an older component would be missed altogether should it be present in the basement of this arc segment.

Geochemical analyses were completed on seven samples from six plutons, with both the outer and middle phases of the Balbuena pluton being analyzed. The purpose of the reconnaissance geochemical survey was initially to test for systematic differences across the aABF and to identify the effects of contraction leading to the peraluminous intrusives of the La Posta event (e.g., Tulloch and Kimbrough, 2003). The results indicate that for the plutons studied the source region(s) and subsequent modifications (e.g. AFC) were generally similar in all respects. All plutons are metaluminous and calc-alkaline with relatively flat, if slightly elevated rare earth element (REE) versus chondrite plots (Fig. 12).

In addition to looking for chemical variations across the aABF, chemical data was collected to look for evidence for the dramatic crustal thickening that drove unique magmatism preceding the La Posta event (Tate and Johnson, 2000; Tulloch and Kimbrough, 2003; Wetmore et al., 2003b). Many of the late Early Cretaceous plutons studied from the eastern part of the Alisitos in the northern Sierra San Pedro Mártir by Tate and Johnson (2000) yield peraluminous, strontium and light REE enriched, and depleted middle and heavy REE compositions. Such chemical compositions are very similar to those of the large La Posta intrusions which are part of the early Late Cretaceous magmatic flare-up that appears to have affected most of the North American Cordilleran margin (e.g., Coleman and Glazner, 1997; Tulloch and Kimbrough, 2003). Tate and Johnson (2000) interpret the chemical signatures of the Sierra San Pedro Mártir plutons to result from the incongruent melting of plagioclase-rich eclogitic lower crust ( $\geq 10$  kbar) with a substantial component of garnet in the residue. Given that all such plutons are late syn to post tectonic in the northern Sierra San Pedro Mártir (Johnson et al., 1999a), all emplaced between 105 and 100 Ma, it is a reasonable interpretation to conclude that this magmatism resulted from pronounced crustal thickening due to contractional event that produced the well formed fold and thrust belt that rims the northern and eastern margins of the Alisitos arc segment (Tate and Johnson, 2000).

As noted above, however, while all of the plutons analyzed for this study are late syn to post tectonic none yield chemical compositions similar to those of similar age from the northern Sierra San Pedro Mártir. Combined with preliminary oxygen isotopic data (Wetmore and Morrison, unpublished data) indicating crustal sources for the intrusives of northern Alisitos arc, these data suggest that crustal thickening in this region was significantly less than that to the south. This interpretation is consistent with observations made when comparing the magnitude of deformation described for the two

regions. Johnson et al. (1999a) describes tight and isoclinal folds with vertical hinge lines present well west of the Main Mártir thrust in the northern Sierra San Pedro Mártir. Conversely, except for some very slight undulations, all hinge lines are subhorizontal south of the aABF (Wetmore et al., in review) indicating considerably less shear in this region when compared with the former. This is also consistent with the difference in the amount of throw across the Main Mártir Thrust relative to the aABF. Metamorphic studies in the region of the Main Mártir Thrust indicate as much 4 kbars of difference between rocks on either side of that fault (Kopf and Whitney, 1999; Schmidt, 2000) while there is likely less than 1.5 kbars difference between the rocks on either side of the aABF given the lack of a metamorphic break coincident with that fault.

### **Road Log**

The mileage for this field trip is measured from the La Pinta Hotel on the corner of Mateo Lopez in Ensenada, Baja California Norte, Mexico. Turn right and head toward Mexican Highway 1 and take it south toward Santo Tomás, and San Vicente. Locations of stops are shown in figures 2 and 3a.

Mi. Km  
23.2 37.4

**STOP 1:** This stop provides an overview of Valle Santo Tomás, formed as a graben between the northern and southern branches of the active Agua Blanca fault. Just before we parked we passed through the damage zone of the northern branch of the fault. Looking south along the western side of the valley are some world class examples of the geomorphology of an active fault system. Several truncated spurs and scarps are clearly observable along the southern branch of the active fault here.

Perhaps more significant to the focus of this field trip, however, is the relationship of this active structure to the Mesozoic ancestral ABF. Subsequent stops will provide you with the opportunity to see the spatial relationship of these two structures, however, the trace of the location of the ancestral structure through this area is still debatable. Mapping (Wetmore and Schultz, unpublished mapping) south of the southern branch of the active ABF has shown that this branch cuts across Cretaceous folds in the Alisitos Formation, near the type section (Allison, 1955, 1974). This indicates that ancestral ABF must be present to the north of this structure but is likely south of the northern branch.

37.2 60.0

Get off Mexican Highway 1 and pass through a cattle guard on the left hand (eastern) side of the road. The road from here to the next stop is a dirt track and requires some moderate ground clearance. There are three forks in the road between the cattle guard and second stop (at 35.7 Mi/60 km, 39.7 Mi/64 km, and 41.1 Mi/66.3 km), bear left at each of these forks.

43.1 69.5

**STOP 2:** This stop includes some of the most easily accessible, if not best, exposures of the ancestral ABF. To the right or south of the road is a small, usually dry, creek at the base of a small hill. The exposures of interest, those of the ancestral ABF, are present within the creek bed and up the north face of the hill at its western end. A newly cut road here may also preserve some additional exposures.

The shear zone here is between 50 and 100 m wide and grades rapidly into brittle-ductily deformed metasediments and volcanics of the Alisitos Formation toward the south. Rocks within the shear zone possess a well formed banding or lithologic layering that is folded and transected by a new crenulation cleavage (Fig. 7b and 7c). The younger foliation forms axial planar to the numerous small folds that form within the older banding. Thin sections of these rocks show quartz is reduced and dynamically recrystallized, while feldspar grains are fractured, and pulled apart with neocrystallized white micas present in the necks.



All mapped exposures of this shear zone are approximately the same distance from the active ABF, 2 to 3 km to the south. The active ABF can be observed from this stop along the hills to the north. Look for tan and purplish colored exposures with rill like drainages. This close spatial relationship may indicate a kinematic or structural link between the two features. However, at present such an interpretation is clearly speculation and requires considerable additional investigation.

49.0 79.0

Take the dirt track back to the highway and turn left on Mexican Highway 1 heading south toward San Vicente.

52.1 84.0

**STOP 3:** (Optional) Stop in the first of two large pullouts along the right or west side of the highway. This is the only stop along Mexican Highway 1 due to the level of danger I associate with this road. Please exercise extreme caution when crossing and standing near the outcrops. Vehicles, especially trucks and buses, do not have much room to spare in this stretch of the highway and will be moving at very high speeds.

Across the road from this pullout are some spectacular exposures of the Alisitos Formation. These road cuts provide an unparalleled opportunity to look at both the component stratigraphy and structure of this part of the Alisitos arc. Present in these exposures are several examples of metavolcanic and volcanoclastic units that typify the Alisitos Formation with lesser argillites also present. While the prominent limestone units described by Silver et al. (1963) are exposed in the hills a few hundred meters north of this stop they are not present in these road cuts. If you are interested in seeing these units walk back up the road to the next bend and look at the hills to the northwest across the small valley. Though often difficult to locate due to weathering and high strains there are some examples of accretionary lapilli within this road cut exposure.

The deformation experienced by these rocks is as obvious as the traffic is fast here. The strata here have been tightly to isoclinally folded causing the nearly vertical attitudes exhibited by these rocks. At this location we are approximately a kilometer south of the El Ranchito fault, a brittle southwest vergent reverse fault, in the heart of a fold and thrust belt.

59.9 96.6

In San Vicente turn left one block past the stop light and Pemex gas station. Drive out of the east side of town, across the abandoned airstrip, and turn left at the grade school. The road from here on will be very difficult and will require some high clearance. Also, there are many sandy areas and these will become potential traps so be prepared as you proceed from this point.

- 63.0 101.6 The road T's at this point, go to the left and into Cañon Agua Caliente. You will be driving up an arroyo very soon after making this turn. As such, the road is a subject to substantial changes from year to year. However, in the recent past it has been best to stay to the right as there are a few active ranches off to the left.
- 65.3 105.3 **STOP 4:** Past a small orange grove (Rancho El Tigre) along the left or northern side of the arroyo are some 10 m high cliffs of steeply dipping metavolcanics. The rocks in this outcrop are on the east limb of an overturned, southwest vergent fold with a steeply east dipping axial plane. Structurally this stop is between the El Ranchito and El Tigre faults, the latter structure is inferred to be ~2 km to the northeast of this stop.  
Present in the metavolcanics at this stop are strongly deformed volcanoclastic units including a block and ash flow tuff. These types of units are ubiquitous throughout the study area and were used to quantify tectonic strains. Units similar to these but undeformed were sampled near the coast at Eréndira and used to correct for the effects of primary or depositional fabrics on the finite fabric ellipsoids (e.g. Wetmore et al., in press in JSG).
- 67.6 109.0 Return to the T in the road and bear left.
- 69.1 111.5 Bear left at a Y in the road.
- 71.4 115.2 **STOP 5:** (Optional) As you start to climb into the hills along this well maintained part of the road you will pass through a relatively continuous section through the Alisitos Formation. At this stop you will have the opportunity to observe the regionally extensive limestone member. This unit can be traced in satellite images from Punta China to the northern Sierra San Pedro Mártir where it is cut out by the Main Mártir thrust. Near Punta China this unit is nearly 100 m thick (Wetmore and Schultz, unpublished mapping), in this area, however, it is characterized by meter scale beds intercalated with metavolcanics and volcanoclastics. In part this is related to ductile strains in addition to initial lateral thickness variations.
- 73.2 118.1 Bear left onto a lesser road leading into an open field. This is officially where the road quality begins to deteriorate.
- 76.3 123.1 **STOP 6:** Before driving back down into Cañon Agua Caliente stop and climb a small hill on the left or south side of the dirt track. Looking north from here the mountains of the Santiago Peak arc segment form the skyline. The low hills in front of the mountains on the skyline are south of Valle Agua Blanca and the active strike slip fault that bears its

name. These hills are held up by a series of intrusive bodies including the Pedrogoso, Arce, and Piedra Rodada. The low area below us here as we look to the west is underlain by the Balbuena pluton, a composite intrusive body that helps constrain the timing of deformation of this part of the Alisitos arc segment. The steep hill directly opposite this hill on the far side of the Balbuena is known as Cerro Calavera. Cerro Calavera is comprised of metaseds and metavolcanics that were folded prior to the intrusion of the Balbuena at ~108.6 Ma. At distances greater than a couple of kilometers from the margin of the Balbuena these folds trend northwest-southeast, but at lesser distances these folds are progressively deflected, counterclockwise, until they strike northeast-southwest at Cerro Calavera. Similar, though antithetic, deflections of host rock structures are observed on the southeastern side of the Balbuena as well.

The Balbuena pluton has also been the subject of considerable study for the ends of constraining its emplacement history. The Balbuena is composed to three phases; outer, middle, and inner (tonalite, diorite, and tonalite, respectively). The middle and outer phases exhibit crescent shapes about the inner phase, though the outer phase is discontinuous. Contact relationships between each of the phases and the surrounding host rocks indicate that the middle phase is the oldest and is likely responsible for the incompletely preserved ~1 km wide structural aureole. Exposures of contacts of the middle phase with the other two phases both show the former phase being disintegrated and incorporated into the latter two phases. In both examples the middle phase appear to have been near its solidus during the intrusion of the other two phases as indicated by rounded and globular shapes of xenoliths. Petrographic observation of the inner and outer phases result in the conclusion that these phases are probably cogenetic and given the apparent high temperature state of the middle phase xenoliths at the contacts it is likely all three phases were emplaced nearly simultaneously. We will look at the contact between the middle and inner phases at the next stop.

- 76.9 124.0 **STOP 7:** After driving down into Cañon Agua Caliente stay on the southeast side of the stream (don't cross the river). Park and walk ~200 m down stream to exposures along the southeast or left side of the cañon. This is a typical exposure of the contact relationships of the middle phase with either the inner or outer phases. Here the relatively felsic inner phase is mechanically incorporating the middle phase, largely through the pervasive intrusion of centimeter scale dikes. Once incorporated some blocks of the middle phase exhibit evidence of progressive in situ disintegration and some appear to have become rounded or globular.

- 89.3 144.0 Make your way back to Highway 1 where you left it. Turn right (north) to head back to Ensenada but for an additional stop turn left (south) toward San Quintin.
- 96.5 155.6 Turn left onto the dirt road to Valle Trinidad. This is a well maintained road that gets plenty of use. However, there are some rough spots here and there.
- 114.7 185.0 **STOP 8:** (Additional) This stop is added on for those interested in the structural and magmatic evolution of the arc. At this stop is a swarm of strongly deformed, even mylonitic, felsic dikes that cut a quartz diorite to tonalite intrusive body. This dike swarm is, in turn, cut out by a gabbro intrusion a few kilometers to the east along this same road (David Kimbrough, personal communication, 2004). The exact age of this dike swarm is not known at present but given that it is cut by a ductile shear zone that can be traced south and connected with the Main Mártir thrust in satellite images it is plausible to assume that they are older than the youngest known slip on that structure (~101 Ma; Johnson et al., 1999a). An upper age limit is not available.
- This dike swarm and those similar to it in the central part of the Peninsular Ranges are becoming of particular interest due to their age and silicic compositions. Dave Kimbrough and students have been studying similar dikes in the Ranch San Marcos and Tres Hermanos region, northeast of Ensenada. Their results show that most dikes are rhyolitic and yield an average age of ~120 Ma (e.g. Böhnel et al., 2002; David Kimbrough, personal communication, 2004). Herzig (1991) reports dikes of similar composition that cut the Bedford Canyon Formation in the Santa Ana Mountains and feed lava flows of the overlying Santiago Peak Volcanics (ages between 123-125 Ma). Johnson et al. (1999a) reports an age of ~127 Ma for a felsic sill(?) or lava flow (now an orthogneiss) present in the hanging wall of the Main Mártir thrust in the northern Sierra San Pedro Mártir. Together, all of these identified dikes of similar age and composition appear to form a continuous belt present along the eastern part of the western and western part of the central Peninsular Ranges. Their temporal and petrologic similarities to those of the preserved sections of the Santiago Peak Volcanics provide a potentially intriguing link that, if convincingly demonstrated, may indicate that the Santiago Peak arc may have existed as far south as the Sierra San Pedro Mártir and perhaps much further.

- Allen, C., L. Silver, and F. Stehil, 1960, Agua Blanca fault--a major transverse structure of northern Baja California, Mexico: *Geological Society of America Bulletin*, v. 71, p. 457-482.
- Allison, E. C., 1955, Middle Cretaceous Gastropoda from Punta China, Baja California, Mexico: *Journal of Paleontology*, v. 29, p. 400-432.
- Allison, E. C., 1974, The type Alisitos Formation (Cretaceous, Aptian-Albian) of Baja California and its bivalve fauna, *in* G. Gastil, and J. Lillegraven, eds., *Geology of peninsular California*, American Association of Petroleum Geologists, Pacific Section, p. 20-59.
- Anderson, C. L., 1991, Zircon uranium-lead isotopic ages of the Santiago Peak Volcanics and spatially-related plutons of the Peninsular Ranges batholith, southern California: M.S. Thesis, San Diego State University, San Diego, California, 111 p.
- Barth, A. P., J. L. Wooden, M. Grove, C. E. Jacobson, and J. N. Pedrick, 2003, U-Pb zircon geochronology of rocks in the Salinas Valley region of California: A reevaluation of the crustal structure and origin of the Salinian block: *Geology*, v. 31, p. 517-520.
- Beggs, J. M., 1984, Volcaniclastic rocks of the Alisitos Group, Baja California, Mexico, *in* V. Frizzell, Jr., ed., *Geology of the Baja California Peninsula*, Society of Economic Paleontologists and Mineralogists, Pacific Section, p. 43-52.
- Böhnel, H., L. A. Delgado-Argote, and D. L. Kimbrough, 2002, Discordant paleomagnetic data for middle-Cretaceous intrusive rocks from northern Baja California: Latitude displacement, tilt or vertical axis rotation?: *Tectonics*, v. 21, p. 1-12.
- Busby, C., D. Smith, W. Morris, and B. Fackler-Adams, 1998, Evolutionary model for convergent margins facing large ocean basins: Mesozoic Baja California, Mexico: *Geology*, v. 26, p. 227-230.
- Carrasco, A. P., D. L. Kimbrough, and C. T. Herzig, 1995, Cretaceous arc-volcanic strata of the western Peninsular Ranges: comparison of the Santiago Peak Volcanics and Alisitos Group: *Abstracts of Peninsular Geological Society International Meeting on Geology of the Baja California Peninsula*, v. III, p. 19.
- Chávez-Cabello, G., 1998, Mecanismos de emplazamiento y evolución magmática de varios plutones al oeste de la Sierra San Pedro Mártir, Baja California, México: Masters thesis, CICESE - Centro de Investigación Científica y de Educación Superior de Ensenada, Ensenada, Baja California Norte, México, 165 p.
- Chou, Y.-W., and H.-S. Yu, 2002, Structural expressions of flexural extension in the arc-continent collisional foredeep of western Taiwan, *in* T. B. Brue, and C.-S. Liu, eds., *Geology and Geophysics of an Arc-Continent Collision*, Taiwan, Boulder, CO, Geological Society of America, p. 1-12.
- Coleman, D. S., and A. F. Glazner, 1997, The Sierra crest magmatic event: rapid formation of juvenile crust during the Late Cretaceous in California: *International Geology Review*, v. 39, p. 768-787.
- DePaolo, D. J., 1981, A neodymium and strontium isotopic study of the Mesozoic calc-alkaline granitic batholiths of the Sierra Nevada and Peninsular Ranges, California: *Journal of Geophysical Research*, v. 86, p. 10,470-10,488.

- Fackler-Adams, B., 1997, Volcanic and sedimentary facies, processes, and tectonics of intra-arc basins: Jurassic continental arc of California and Cretaceous oceanic arc of Baja California: Ph.D. thesis, University of California at Santa Barbara, Santa Barbara, California, 248 p.
- Fackler-Adams, B. N., and Busby, C.J., 1998, Structural and stratigraphic evolution of extensional oceanic arcs: *Geology*, v. 26, p. 735-738.
- Gastil, R. G., 1993, Prebatholithic history of Peninsular California, *in* R. G. Gastil, and R. H. Miller, eds., *The Prebatholithic Stratigraphy of Peninsular California*, Geological Society of America Special Paper, v. 279, p. 145-156.
- Gastil, R. G., C. K. Diamond, M. J. Walawender, M. Marshal, C. Boyles, and B. Chadwick, 1990, The problem of the magnetite/ilmenite boundary in southern and Baja California, *in* J. L. Anderson, ed., *The Nature and Origin of Cordilleran Magmatism*, Boulder, CO, Geological Society of America Memoir, v. 174, p. 19-32.
- Gastil, R. G., and M. S. Girty, 1993, A reconnaissance U-Pb study of detrital zircon in sandstones of peninsular California and adjacent areas, *in* R. G. Gastil, and R. H. Miller, eds., *The Prebatholithic Stratigraphy of Peninsular California*, Geological Society of America Special Paper, v. 279 p. 135-144.
- Gastil, R. G., G. J. Morgan, and D. Krummenacher, 1981, The tectonic history of peninsular California and adjacent Mexico, *in* W. G. Ernst, ed., *The geotectonic development of California*, Englewood Cliffs, New Jersey, Prentice-Hall, p. 284-306.
- Gastil, R. G., R. Phillips, and E. Allison, 1975, Reconnaissance geology of the State of Baja California: Geological Society America, v. Memoir 140, 170 pp.
- Gehrels, G. E., J. H. Stewart, and K. B. Ketner, 2002, Cordilleran-margin quartzites in Baja California -- Implications for tectonic transport: *Earth and Planetary Science Letters*, v. 199, p. 201-210.
- Griffith, R., and J. Hoobs, 1993, Geology of the southern Sierra Calamajue, Baja California Norte, Mexico, *in* R. G. Gastil, and R. H. Miller, eds., *The Prebatholithic Stratigraphy of Peninsular California*, Geological Society of America Special Paper, v. 279, p. 43-60.
- Gromet, L. P., and Silver, L.T., 1987, REE variations across the Peninsular Ranges batholith: Implications for batholithic petrogenesis and crustal growth in magmatic arcs: *Journal of Petrology*, v. 28, p. 75-125.
- Hall, C. A., 1991, Geology of the Point Sur-Lopez Point region, Coast Ranges, California: A part of the Southern California allochthon: Geological Society of America Special Paper, v. 266, p. 40 p.
- Herzig, C. T., 1991, Petrogenetic and tectonic development of the Santiago Peak Volcanics, northern Santa Ana Mountains, California: Ph.D. thesis, U.C. Riverside, Riverside, California, 376 p.
- Hossack, J. R., 1968, Pebble deformation and thrusting in the Bygdin area (southern Norway): *Tectonophysics*, v. 5, p. 315-339.
- Johnson, S. E., J. M. Fletcher, C. M. Fanning, S. R. Paterson, R. H. Vernon, and M. C. Tate, 2003, Structure and emplacement of the San Jose tonalite pluton, Peninsular Ranges batholith, Baja California, Mexico: *Journal of Structural Geology*, v. 25, p. 1,933-1,957.

- Johnson, S. E., S. R. Paterson, and C. M. Tate, 1999, Structure and emplacement history of a multiple-center, cone-sheet-bearing ring complex: The Zarza intrusive complex, Baja California, Mexico: *Geological Society of America Bulletin*, v. 111, p. 607-619.
- Johnson, S. E., M. C. Tate, and C. M. Fanning, 1999, New geologic mapping and SHRIMP U-Pb data in the Peninsular Ranges batholith, Baja California, Mexico: Evidence of a suture?: *Geology*, v. 27, p. 743-746.
- Kopf, C. F., and D. L. Whitney, 1999, Variation in metamorphic grade across a possible inter-arc convergent boundary, Peninsular Ranges, Mexico: *Geological Society of America Abstracts with Programs*, v. 31, p. 294.
- Legg, M. R., O. V. Wong, and F. Suarez-Vidal, 1991, Geologic structure and tectonics of the inner continental borderland of northern Baja California, *in* J. P. E. Dauphin, and B. R. T. Simoneit, eds., *The Gulf and Peninsular Province of the Californias*, Tulsa, OK, p. 145-177.
- Lundberg, N., D. L. Reed, C.-S. Liu, and J. H. Lieskes, Jr., 1997, Forearc-basin closure and arc accretion in the submarine suture zone south of Taiwan: *Tectonophysics*, v. 274, p. 5-24.
- Marsaglia, K. M., 1995, Interarc and backarc basins, *in* C. Busby, and R. Ingersoll, eds., *Tectonics of Sedimentary Basins*, Blackwell, p. 299-329.
- Miller, D. M., and G. Oertel, 1979, Strain determination from the measurement of pebble shapes: a modification: *Tectonophysics*, v. 55, p. T11-T13.
- Molnar, P., and T. Atwater, 1978, Interarc spreading and Cordilleran tectonics as alternates related to age of subducted oceanic lithosphere: *Earth and Planetary Science Letters*, v. 41, p. 330-340.
- Premo, W. R., D. M. Morton, L. W. Snee, C. M. Fanning, and N. D. Naeser, 1998, Isotopic ages, cooling histories, and magmatic origins for Mesozoic tonalitic plutons from the northern Peninsular Ranges batholith, southern California: *Geological Society of America Abstracts with Program*, v. 30, p. 59-60.
- Schmidt, K. L., 2000, Investigations of arc processes: relationships among deformation magmatism, mountain building, and the role of crustal anisotropy in the evolution of the Peninsular Ranges batholith, Baja California: Ph.D. thesis, University of Southern California, Los Angeles, CA, 324 p.
- Shimamoto, T., and Y. Ikeda, 1976, A simple algebraic method for strain estimation from deformed ellipsoidal objects. 1. Basic theory: *Tectonophysics*, v. 36, p. 315-337.
- Silver, L. T., Stehli, G.G., and Allen, C.R., 1963, Lower Cretaceous pre-batholithic rocks of northern Baja California, Mexico: *Bulletin of the American Association of Petroleum Geologists*, v. 47, p. 2054-2059.
- Silver, L. T., and Chappell, B.W., 1988, The Peninsular Ranges Batholith: an insight into the evolution of the Cordilleran batholiths of southwestern North America: *Transactions of the Royal Society of Edinburgh*, v. 79, p. 105-121.
- Suarez-Vidal, F., 1986, Alisitos Formation calcareous facies: Early Cretaceous episode of tectonic calm: *American Association of Petroleum Geologists Bulletin*, v. 70, p. 480.
- Suarez-Vidal, F., R. Armijo, G. Morgan, P. Bodin, and R. G. Gastil, 1991, Framework of recent and active faulting in northern Baja California, *in* J. P. E. Dauphin, and B. R. T. Simoneit, eds., *The Gulf and Peninsular Province of the Californias*, Tulsa, OK, p. 285-300.

- Suppe, J., 1970, Offset of late Mesozoic basement terrains by the San Andreas fault system: Geological Society of America Bulletin, v. 81, p. 3,253-3,258.
- Sutherland, M., P. H. Wetmore, C. Herzig, and S. R. Paterson, 2002, The Early Cretaceous Santiago Peak arc: A continental margin arc built on the North American Triassic-Jurassic accretionary prism of southern and Baja California: Geological Society of America Abstracts with Programs, v. 34, p. 43.
- Tate, M. C., and S. E. Johnson, 2000, Subvolcanic and deep-crustal tonalite genesis beneath the Mexican Peninsular Ranges: Journal of Geology, v. 108, p. 720-728.
- Tate, M. C., M. D. Norman, S. E. Johnson, C. M. Fanning, and J. L. Anderson, 1999, Generation of tonalite and trondhjemite by subvolcanic fractionation and partial melting in the Zarza Intrusive Complex, western Peninsular Ranges batholith, northwestern Mexico: Journal of Petrology, v. 40, p. 983-1,010.
- Taylor, H. P. J., and L. T. Silver, 1978, Oxygen isotope relationships in plutonic igneous rocks of the Peninsular Ranges batholith, southern and Baja California, *in* R. E. Zartman, ed., Short papers of the fourth international conferences on geochronology, p. 423-426.
- Tulloch, A. J., and D. L. Kimbrough, 2003, Paired plutonic belts in convergent margins and the development of high Sr/Y magmatism: Peninsular Ranges batholith of Baja-California and Median batholith of New Zealand, *in* S. E. Johnson, S. R. Paterson, J. M. Fletcher, G. H. Girty, D. L. Kimbrough, and A. Martin-Barajas, eds., Tectonic evolution of northwestern Mexico and the southwestern USA, Boulder, CO, Geological Society of America, p. 275-296.
- Wetmore, P. H., and S. R. Paterson, 2002, Primary grain shapes and grain preferred orientations: Why no analysis of finite strain is complete without their incorporation: EOS Transactions AGU, v. 83, p. 613.
- Wetmore, P. H., K. L. Schmidt, and S. R. Paterson, 2001, Amnesia in pluton emplacement, Balbuena pluton, Baja California, Mexico: Geological Society of America Abstracts with Programs, v. 33, p. 325.
- Wetmore, P. H., K. L. Schmidt, S. R. Paterson, and C. Herzig, 2002, Tectonic implications for the along-strike variation of the Peninsular Ranges batholith, southern and Baja California: Geology, v. 30, p. 247-250.
- Wetmore, P. H., C. Herzig, P. W. Schultz, H. Alsleben, M. Sutherland, S. R. Paterson, and K. L. Schmidt, 2003, Mesozoic tectonic evolution of the Peninsular Ranges of southern Baja California, *in* S. E. Johnson, S. R. Paterson, J. M. Fletcher, G. H. Girty, D. L. Kimbrough, and A. Martin-Barajas, eds., Tectonic evolution of northwestern Mexico and the southwestern USA, Boulder, CO, Geological Society of America, p. 93-116.
- Wetmore, P. H., M. Ducea, G. Gehrels, K. L. Schmidt, and S. R. Paterson, 2003b, Magmatic response to differential crustal thickening: Geochemical constraints on the tectonic evolution of the Alisitos arc segment of Baja California, Mexico: Geological Society of America Abstracts with Programs, v. 35, p. 45-10.



Figure 1. Regional map of the Peninsular Ranges of southern and Baja California showing distribution of various stratigraphic units and locations discussed in the text. Numbered locations correspond to 1) Santa Ana Mountains, 2) Lusardi Canyon, 3) Punta China, 4) Eréndira, 5) northern Sierra San Pedro Mártir (study area for Johnson et al., 1999a,b, and 2003; Tate et al., 1999; Tate and Johnson, 2000), 6) southern Sierra San Pedro Mártir (study area for Schmidt, 2000; Schmidt and Paterson, 2003), 7) Sierra Calamajue. Figure is modified after Gastil (1993), and 8) San Matias Pass.

Figure 2. Geologic map of the ancestral Agua Blanca fault region. Box shows outline of detailed map area depicted in Figure 3.

Figure 3. Detailed geologic map of the ancestral Agua Blanca fault region. a) Map showing bedding with stereoplots of all bedding attitudes broken out for the two arc segments and stops for this field trip. Also shown are stereoplots of poles to bedding for both the Santiago Peak Volcanics and the Alisitos Fm. Mean principle orientation represents bedding orientation and not the poles to bedding. b) Map showing subsolidus foliations with stereoplots of poles to the foliation broken out for the two arc segments. Mean principle orientation represents foliation orientation and not the poles to foliation. c) Map showing subsolidus lineations with stereoplots of broken out for the two arc segments. d) Map showing YZ plane of the strain ellipsoids calculated in this study. Ellipses are plotted with actual orientations and number inside each ellipse represents the magnitude of the x-axis relative to the z-axis at unity. The line shown in this map is that used in the block diagram of figure 3e. e) Block diagram of the section shown in figure 3d showing major structures and the XZ plane of the strain ellipsoids calculated in this study. Ellipses are plotted with actual orientations and numbers shown at the lower left of each ellipse represent the magnitude of the y-axis relative to the z-axis as unity.

Figure 4. Stratigraphic column for the Alisitos Formation in the central part of the ancestral Agua Blanca fault study area. The XZ plane of the strain ellipsoids calculated in this study are also shown. While orientations relatively to bedding are not accurately plotted, the z-axis of most ellipsoids are oriented normal to bedding planes.

Figure 5. Geologic map of the ancestral Agua Blanca fault study area showing sample locations. Table 1 relates the sample number shown on map to sample name. See Figure 2 for symbol key.

Figure 6. Relative age probability plot of U/Pb ages of detrital zircons for samples 6/6/00-F and 5/19/00-A from the Alisitos Formation.

Figure 7. a) Field photo of the El Ranchito fault in Cañon El Trigo looking northwest. b) Photomicrograph of a thin section from a sample of the ancestral Agua Blanca fault view to the southeast. Primary, continuous, foliation dips steeply to the left in this photo and the second, crenulation, foliation dips steeply to the right. c) Field photo of the ancestral Agua Blanca fault from western-most exposure looking to the southeast. Note the primary foliation dipping steeply to the left, (northeast) parallel to the marker, is folded in the bottom center of the photo.

Figure 8. Modified Flinn diagram of strain data from the ancestral Agua Blanca fault region.

Fig. 9. Three plots of different aspects of strain at distances relative to the ancestral Agua Blanca fault. Does not include samples clearly affected by pluton emplacement related deformation. The Lode's parameter describes ellipsoid shape and is equal to  $(2\varepsilon_2 - \varepsilon_1 - \varepsilon_3)/(\varepsilon_1 - \varepsilon_3)$ , where  $\varepsilon$  is equal the natural or logarithmic strain (Hossack, 1968). Ellipsoids with a Lode's parameter less than zero is prolate and greater than zero is oblate.

Figure 10. a) Field photo of a microgranitoid enclave from within the portion of the Piedra Rodada pluton characterized by subsolidus deformation. Photo is taken looking northwest at a plane that is normal to the foliation and parallel to the lineation. The asymmetry exhibited by the enclave suggests a top to the southwest sense of shear. b) Field photo of the Piedra Rodada pluton <50 m from the ancestral Agua Blanca fault looking northwest. Here a strong subsolidus fabric exhibits an asymmetric fold indicating a top to the southwest sense of shear. c) Field photo of the small fault southwest of the El Ranchito fault looking to the northwest. Small drag folds formed below the fault suggest a top to the southwest sense of shear.

Figure 11. Plots of all U/Pb zircon age data collected from the six plutons analyzed in this study. Uncertainties for individual analyses are shown at the 1-sigma level. Reported ages are based on the weighted mean, with 2-sigma uncertainties shown for random error (mean) and for the quadratic sum of random and systematic error (age).

Figure 12. Plot of chondrite-normalized rare earth element abundances for plutons from the ancestral Agua Blanca fault study area.

Figure 13. Schematic model of the inferred accretion of the Alisitos arc segment to the continental margin during the Early Cretaceous illustrating the potential relative convergence direction to explain deformation gradient and sinistral shear observed in the aABF region.

Table 1. List of samples collected and analyzed from the ancestral Agua Blanca fault study area. Location number corresponds to the map in Figure 4.

PHW Sample	Loc. Number	Strain	Geochron	Geochem
6/6/00-F	1		x	
5/19/00-A	2		x	
2/24/01-A	3	X		
2/24/01-B1	3	X		
2/24/01-B2	3	X		
2/24/01-B3	3	X		
2/24/01-B4	3	X		
2/24/01-B6	3	X		
2/24/01-C	3	X		
2/24/01-C1	3	X		
5/21/00-C	4	X		
5/26/00-C	5	X		
6/9/00-D	6	X		
6/9/00-I	6	X		
6/13/00-E	7	X		
6/13/00-F	7	X		
6/22/00-B	4	X		
6/22/00-M	8	X		
5/7/01-J	9	X		
5/17/01-P	10	X		
6/5/01-A	9	X		
6/6/01-H	11	X		
6/6/01-N	12	X		
6/24/01-J	13	X		
6/25/01-G	14	X		
6/25/01-H	14	X		
7/6/01-T	15	X		
5/29/01-B	16		X	X
1/8/03-H	17		X	X
7/3/01-J	18			X
7/1/01-F	19			X
7/6/01-S	20		X	
6/9/01-B	21		X	X
6/9/01-F	22		X	X
1/12/03-A	23		X	X

Table 3. Whole rock geochemical data for plutonic samples collected from the ancestral Agua Blanca fault study area.

Samples	5/29/01-B Santo Tomas Pluton	1/8/03-H Agua Blanca Pluton	7/3/01-J Arce Pluton	7/1/01-F Piedra Rodado	6/9/01-B Balbuena Phase II	6/9/01-F Phase III Balbuena	1/12/03-A San Vicente Pluton
<b>SiO<sub>2</sub></b>	69.61	74.01	71.55	62.89	72.99	58.16	62.69
<b>TiO<sub>2</sub></b>	0.520	0.215	0.431	0.679	0.317	1.067	0.530
<b>Al<sub>2</sub>O<sub>3</sub></b>	13.85	12.48	13.62	15.42	13.85	16.59	16.74
<b>FeO</b>	ND	ND	ND	ND	ND	ND	ND
<b>Fe<sub>2</sub>O<sub>3</sub></b>	4.20	2.61	2.69	6.07	2.87	8.39	5.64
<b>MnO</b>	0.064	0.101	0.055	0.110	0.081	0.173	0.112
<b>MgO</b>	0.87	0.17	0.62	2.30	0.52	3.12	2.26
<b>CaO</b>	2.95	0.90	2.56	4.68	2.50	6.13	5.57
<b>Na<sub>2</sub>O</b>	4.37	4.42	4.17	3.51	4.64	3.60	3.70
<b>K<sub>2</sub>O</b>	1.37	2.84	2.64	1.88	1.65	0.72	0.76
<b>P<sub>2</sub>O<sub>5</sub></b>	0.13	0.04	0.09	0.14	0.08	0.21	0.13
<b>LOI</b>	0.55	0.97	0.73	1.02	0.72	0.87	1.43
<b>TOTAL</b>	98.50	98.76	99.15	98.70	100.22	99.02	99.55
Trace Elements (ppm)							
<b>Ba</b>	426	756	715	503	448	267	278
<b>Rb</b>	34	48	30	57	42	17	18
<b>Sr</b>	209	87	177	209	155	295	327
<b>Y</b>	24	86	52	33	24	29	12
<b>Zr</b>	242	232	274	159	161	114	65
<b>Nb</b>	5	7	9	5	5	5	3
<b>Th</b>	7.8	7.3	7.0	11.7	4.4	2.5	2.0
<b>Pb</b>	11	17	13	7	8	6	7
<b>Ga</b>	17	19	17	17	15	18	19
<b>V</b>	37	25	20	100	18	144	89
<b>Hf</b>	6.6	7.0	8.0	5.2	4.8	3.5	2.2
<b>Cs</b>	1.8	0.5	0.5	1.1	1.7	0.8	0.7
<b>Sc</b>	7	9	15	7	19	9	6
<b>Ta</b>	0.4	0.6	0.8	0.4	0.4	0.3	0.2
<b>U</b>	1.9	2.2	2.3	1.8	1.2	0.8	0.6
<b>Sn</b>	2	3	4	3	6	2	4
<b>Be</b>	1	2	1	2	1	BDL	2
<b>Zn</b>	88	137	80	86	71	93	79
<b>Ge</b>	1	2	2	1	2	BDL	1
<b>Tm</b>	0.41	1.43	0.80	0.56	0.41	0.47	0.20
<b>W</b>	7	17	11	5	6	3	14
<b>Tl</b>	0.3	0.4	0.2	0.3	0.3	0.1	BDL

Table 2. Strain data collected from volcanoclastic rocks throughout the Alisitos arc. Elongations are apparent constant volume extensions and assume that the final axial ratios (X,Y,Z) formed by constant volume strain of an initially perfectly uniform population of markers with initial axial lengths equal to  $L_0$ . Natural strains are the natural logarithms of the ratio for each axial length to the initial axial length. Strain intensity is equal to  $1/3[(E_1-E_2)^2+(E_1-E_3)^2+(E_3-E_1)^2]^{1/2}$  where  $E_x$  are the principal natural strains (Hossack, 1968). Symmetry is equivalent to the Lode's parameter (LP<0 is prolate, LP=0 is plane strain, and LP>0 is oblate). PHW samples are from the aABF study area (Fig. 5). PWS samples are from an area between Santo Tomás and Punta China (Schultz and Wetmore, unpublished mapping). BC and Chavez samples are from the northern Sierra San Pedro Mártir (Johnson et al., 1999b; Chavez-Cabello, 1998). Griffith samples are from the Sierra Calamajue (Griffith and Hoobs, 1993) and SP samples are from the southern Sierra San Pedro Mártir (Schmidt, 2000).

Sample	Lengths			Lo	Elongations			Natural Strains			Strain Intensity	Lodes Parameter
	X	Y	Z		X	Y	Z	X	Y	Z		
PHW 2/24/01-A	1.29	1.21	1.00	1.16	11.29	4.28	-13.84	0.11	0.04	-0.15	0.19	0.49
PHW 2/24/01-B1	1.12	1.03	1.00	1.05	6.67	-1.94	-4.40	0.06	-0.02	-0.05	0.08	-0.54
PHW 2/24/01-B2	1.21	1.10	1.00	1.10	9.78	0.20	-9.09	0.09	0.00	-0.10	0.13	0.03
PHW 2/24/01-B3	1.62	1.49	1.00	1.34	20.63	11.13	-25.41	0.19	0.11	-0.29	0.36	0.66
PHW 2/24/01-B4	1.39	1.16	1.00	1.17	18.62	-1.01	-14.84	0.17	-0.01	-0.16	0.24	-0.09
PHW 2/24/01-B6	1.19	1.13	1.00	1.10	7.62	2.28	-9.16	0.07	0.02	-0.10	0.12	0.40
PHW 2/24/01-C	1.36	1.24	1.00	1.19	14.33	4.26	-16.10	0.13	0.04	-0.18	0.23	0.40
PHW 2/24/01-C1	1.18	1.14	1.00	1.10	7.01	3.07	-9.33	0.07	0.03	-0.10	0.12	0.55
PHW 5/17/01-P	1.57	1.29	1.00	1.27	24.40	1.71	-20.97	0.22	0.02	-0.24	0.32	0.00
PHW 5/21/00-C	2.30	1.44	1.00	1.49	54.39	-3.59	-32.82	0.43	-0.04	-0.40	0.59	-0.33
PHW 5/26/00-C	6.91	3.18	1.00	2.80	146.68	13.56	-64.30	0.90	0.13	-1.03	1.38	-0.26
PHW 5/7/01-J	3.80	2.77	1.00	2.19	73.39	26.39	-54.37	0.55	0.23	-0.78	0.57	0.26
PHW 5/9/00-C	6.66	4.14	1.00	3.02	120.46	37.05	-66.90	0.79	0.32	-1.11	1.40	0.11
PHW 6/13/00-E	4.68	2.15	1.00	2.16	116.65	-0.31	-53.70	0.77	0.00	-0.77	1.09	-0.37
PHW 6/13/00-F	9.92	3.04	1.00	3.11	218.61	-2.29	-67.88	1.16	-0.02	-1.14	1.62	-0.54
PHW 6/22/00-B	2.34	1.46	1.00	1.50	55.55	-3.25	-33.55	0.44	-0.03	-0.41	0.60	-0.32
PHW 6/22/00-M	6.16	4.30	1.00	2.98	106.68	44.15	-66.44	0.73	0.37	-1.09	1.36	0.28
PHW 6/24/01-J	3.18	2.32	1.00	1.95	63.43	19.09	-48.62	0.49	0.17	-0.67	0.85	0.21
PHW 6/25/01-G	15.00	10.00	1.00	5.31	182.31	88.21	-81.18	1.04	0.63	-1.67	1.19	0.29
PHW 6/25/01-H	27.00	6.00	1.00	5.45	395.29	10.06	-81.66	1.60	0.10	-1.70	1.35	-0.62
PHW 6/5/01-A	4.20	3.27	1.00	2.40	75.31	36.66	-58.26	0.56	0.31	-0.87	1.08	0.42
PHW 6/6/01-H	3.21	2.54	1.00	2.01	59.64	26.04	-50.30	0.47	0.23	-0.70	0.87	0.39
PHW 6/6/01-N	2.96	2.26	1.00	1.88	57.08	19.84	-46.88	0.45	0.18	-0.63	0.80	0.28
PHW 6/7/00-C	4.09	3.59	1.00	2.45	67.05	46.68	-59.19	0.51	0.38	-0.90	1.10	0.68
PHW 6/9/00-D	1.55	1.35	1.00	1.28	21.30	5.34	-21.74	0.19	0.05	-0.25	0.32	0.26
PHW 6/9/00-I	3.88	2.77	1.00	2.21	75.91	25.42	-54.67	0.56	0.23	-0.79	1.00	0.23
PHW 7/6/01-T	9.68	4.49	1.00	3.52	175.30	27.68	-71.55	1.01	0.24	-1.26	1.63	-0.20
PWS 1-9-E	1.31	1.16	1.00	1.15	14.14	0.85	-13.13	0.13	0.01	-0.14	0.19	0.03
PWS 2-24-E	1.54	1.38	1.00	1.29	20.08	7.09	-22.23	0.18	0.07	-0.25	0.32	0.39
PWS 2-24-D	1.56	1.41	1.00	1.30	20.12	8.19	-23.05	0.18	0.08	-0.26	0.33	0.45
PWS 2-24-B	1.65	1.26	1.00	1.28	29.33	-1.41	-21.57	0.26	-0.01	-0.24	0.35	-0.21
PWS 2-23-C	1.63	1.44	1.00	1.33	22.67	8.38	-24.79	0.20	0.08	-0.28	0.36	0.40
PWS 1-10-I	1.14	1.06	1.00	1.06	7.00	-0.52	-6.06	0.07	-0.01	-0.06	0.09	-0.15
PWS 9-23-H	1.54	1.38	1.00	1.29	19.83	7.31	-22.24	0.18	0.07	-0.25	0.32	0.40

Sample	Lengths			Lo	Elongations			Natural Strains			Strain	Lodes
	X	Y	Z		X	Y	Z	X	Y	Z	Intensity	Parameter
<b>BC 207</b>	2.19	1.90	1.00	1.61	36.16	18.13	-37.83	0.31	0.17	-0.48	0.59	0.51
<b>BC 208</b>	3.56	2.96	1.00	2.19	62.38	35.01	-54.39	0.48	0.30	-0.78	0.97	0.53
<b>BC 209</b>	7.12	3.53	1.00	2.93	143.07	20.51	-65.86	0.89	0.19	-1.07	1.41	-0.17
<b>BC 220</b>	1.46	1.26	1.00	1.23	19.15	2.83	-18.39	0.18	0.03	-0.20	0.27	0.13
<b>BC 221</b>	1.27	1.12	1.00	1.12	13.03	-0.59	-11.00	0.12	-0.01	-0.12	0.17	-0.13
<b>BC 387</b>	2.33	2.00	1.00	1.67	39.50	19.74	-40.13	0.33	0.18	-0.51	0.64	0.50
<b>BC 413</b>	1.48	1.11	1.00	1.18	25.43	-5.93	-15.25	0.23	-0.06	-0.17	0.29	-0.54
<b>BC 472</b>	6.48	6.33	1.00	3.45	87.90	83.55	-71.00	0.63	0.61	-1.24	1.52	0.95
<b>BC 506A</b>	4.45	2.63	1.00	2.27	96.00	15.84	-55.96	0.67	0.15	-0.82	0.92	-0.06
<b>Chavez PP-1</b>	1.34	1.26	1.00	1.19	12.38	5.89	-15.96	0.12	0.06	-0.17	0.13	0.54
<b>Chavez PP-2</b>	3.77	2.42	1.00	2.09	80.24	15.92	-52.14	0.59	0.15	-0.74	0.55	0.03
<b>Chavez PP-3</b>	4.44	3.79	1.00	2.56	73.38	47.79	-60.97	0.55	0.39	-0.94	0.67	0.62
<b>Chavez SPM-1</b>	14.07	4.61	1.00	4.02	250.24	14.72	-75.11	1.25	0.14	-1.39	1.08	-0.45
<b>Griffith-154</b>	5.24	3.07	1.00	2.52	107.63	21.50	-60.36	0.73	0.19	-0.93	0.69	-0.03
<b>Griffith-158</b>	5.32	2.67	1.00	2.42	119.58	10.29	-58.71	0.79	0.10	-0.88	0.69	-0.23
<b>Griffith-158A</b>	7.08	2.98	1.00	2.76	156.31	7.81	-63.81	0.94	0.08	-1.02	0.80	-0.35
<b>SP 100</b>	6.20	2.81	1.00	2.59	139.15	8.32	-61.40	0.87	0.08	-0.95	1.30	-0.30
<b>SP 137-B</b>	2.12	1.83	1.00	1.57	34.71	16.55	-36.31	0.30	0.15	-0.45	0.02	0.49
<b>SP 548-B</b>	4.51	2.73	1.00	2.31	95.32	18.14	-56.66	0.67	0.17	-0.84	1.01	-0.02
<b>SP 801</b>	6.35	3.75	1.00	2.88	120.60	30.38	-65.23	0.79	0.27	-1.06	1.18	0.03
<b>SP 806</b>	4.29	2.86	1.00	2.31	85.77	24.16	-56.65	0.62	0.22	-0.84	1.02	0.13
<b>SP 828</b>	4.44	3.94	1.00	2.60	70.97	51.82	-61.48	0.54	0.42	-0.95	1.00	0.71
<b>SP 902</b>	2.83	2.02	1.00	1.79	58.52	12.75	-44.05	0.46	0.12	-0.58	0.75	0.11
<b>SP 99</b>	6.87	1.53	1.00	2.19	213.45	-30.07	-54.38	1.14	-0.36	-0.78	1.82	-0.82

Table 3. Continued

Samples	5/29/01-B	1/8/03-H	7/3/01-J	7/1/01-F	6/9/01-B	6/9/01-F	1/12/03-A
Description	Santo Tomas Pluton	Agua Blanca Pluton	Arce Pluton	Piedra Rodado	Balbuena Phase II	Phase III Balbuena	San Vicente Pluton
Rare Earth Elements (ppm)							
La	17.9	14.4	17.6	23.9	15.0	15.2	7.4
Ce	36.6	34.1	55.6	48.1	31.2	32.7	15.6
Pr	4.16	5.73	7.01	5.43	3.80	3.97	1.94
Nd	17.1	30.5	28.8	22.2	16.4	17.3	8.4
Sm	3.9	9.7	6.9	5.3	3.8	4.6	2.2
Eu	1.62	1.11	1.50	1.25	1.01	1.54	0.79
Gd	3.8	11.4	7.0	5.2	3.5	4.8	2.1
Tb	0.7	2.2	1.3	1.0	0.7	0.9	0.4
Dy	4.0	13.9	8.2	5.6	4.0	5.2	2.1
Ho	0.8	3.0	1.8	1.2	0.8	1.0	0.4
Er	2.6	9.1	5.3	3.6	2.5	3.1	1.2
Yb	2.9	9.5	5.4	3.6	2.9	3.0	1.3
Lu	0.46	1.41	0.84	0.54	0.45	0.44	0.20

Table 4. Radiogenic isotopic data for plutonic samples collected from the ancestral Agua Blanca fault study area.

Samples	5/29/01-B	1/8/03-H	7/3/01-J	7/1/01-F	6/9/01-B	6/9/01-F	1/12/03-A
Description	Santo Tomas Pluton	Agua Blanca Pluton	Arce Pluton	Piedra Rodada	Balbuena Phase II	Phase III Balbuena	San Vicente Pluton
Sm (ppm)	2.57	3.05	5.13	3.99	2.91	2.86	1.56
Nd (ppm)	11.38	12.35	23.36	18.41	12.45	12.61	6.61
Sm/Nd	0.226	0.228	0.219	0.217	0.233	0.226	0.235
$^{147}\text{Sm}/^{144}\text{Nd}$	0.1365	0.1387	0.1327	0.1311	0.1412	0.1371	0.1423
$^{143}\text{Nd}/^{144}\text{Nd}$ (0)	0.5129	0.5129	0.5129	0.5129	0.5129	0.5129	0.5129
$\epsilon$ Nd (0)	5.26	5.01	4.93	4.5	5.47	5.3	5.31
$^{143}\text{Nd}/^{144}\text{Nd}$ (100)	0.5128	0.5128	0.5128	0.5128	0.5128	0.5128	0.5128
$\epsilon$ Nd (100)	6.03	6	5.75	5.34	6.17	6.06	6
Rb (ppm)	33.01	45.88	28.37	43.83	16.04	40.93	16.53
Sr (ppm)	207.3	82.6	168.1	205.7	278.9	152.3	310.8
$^{87}\text{Rb}/^{86}\text{Sr}$	0.4604	1.6062	0.4881	0.6163	0.1664	0.7775	0.1538
$^{87}\text{Sr}/^{86}\text{Sr}$ (0)	0.7040	0.7059	0.7040	0.7046	0.7035	0.7043	0.7036
$^{87}\text{Sr}/^{86}\text{Sr}$ (100)	0.7034	0.7035	0.7033	0.7037	0.7033	0.7032	0.7034
$^{206}\text{Pb}/^{238}\text{U}$ (age Ma)	$115 \pm 3.9$	$116 \pm 3.8$		$105.5 \pm 3.4$	$107.7 \pm 3.6$	$108.6 \pm 3.96$	$105.0 \pm 3.4$

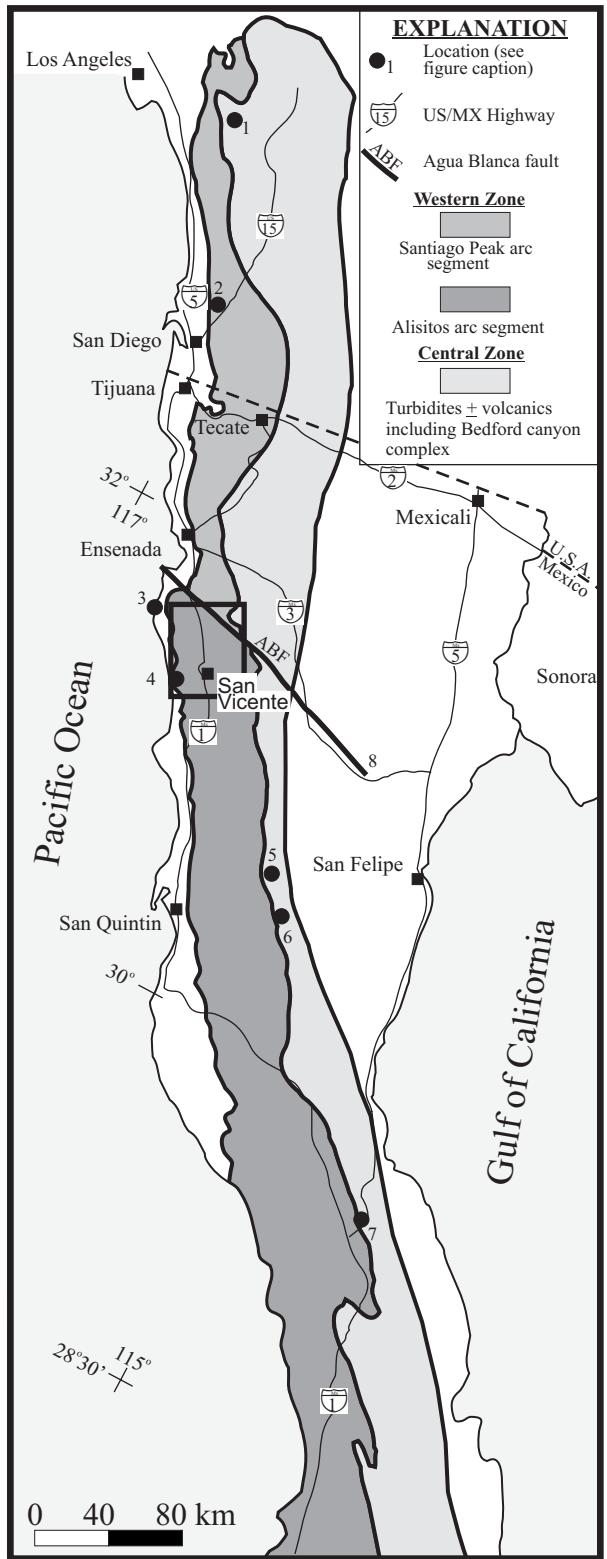









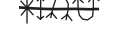

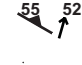




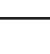



Figure 1.





Figure 2 Continued.

<b>Map symbol and unit key for Figs. 2, 3, and 5</b>	
	Plutons: Undifferentiated figs. 2 and 5, tonalites, gabbro/diorites, mixed.
	Santiago Peak Volcanics
	Alisitos Formation: undifferentiated or volcanic-rich, volcanoclastics-rich
	Alisitos Formation, Limestones (marbles)
	Ancestral Agua Blanca fault
	Secondary thrust faults
	Active Agua Blanca fault
	Secondary strike slip faults
	Normal faults
	Folds: syncline, anticline overturned syncline, overturned anticline
	Bedding symbols with dip angle
	Subsolidus foliations and lineations
	Phase boundaries in plutons
	Trend lines of bedding traces
	Ranches
	Mexican highway 1
	Secondary paved road
	Strain ellipse (YZ fig. 3d, XZ fig. 3e). Number is ratio of the third axis relative to the Z-axis (e.g., X/Z fig. 3d).
<b>KAF<sub>mv/ms</sub></b>	Alisitos Fm. Metavolcanics Metasediments
<b>KST</b>	Santo Tomas pluton
<b>KZ</b>	Zacaton pluton
<b>KAL</b>	El Aleman pluton
<b>KAB</b>	Agua Blanca pluton
<b>KPC</b>	Paredes Coloradas pluton
<b>KP</b>	Pedrogoso pluton
<b>KA</b>	Arce pluton
<b>KSJ</b>	San Jacinto pluton
<b>KET</b>	El Trigo pluton
<b>KPR</b>	Piedra Rodada pluton
<b>KTJ</b>	Trondhjemite dike
<b>KG</b>	El Gigante pluton
<b>KBP</b>	Balbuena pluton
<b>KLA</b>	Los Alamos pluton
<b>KSV</b>	San Vicente pluton
<b>KDT</b>	Dos Tortas pluton
<b>KLC</b>	Los Cochis pluton

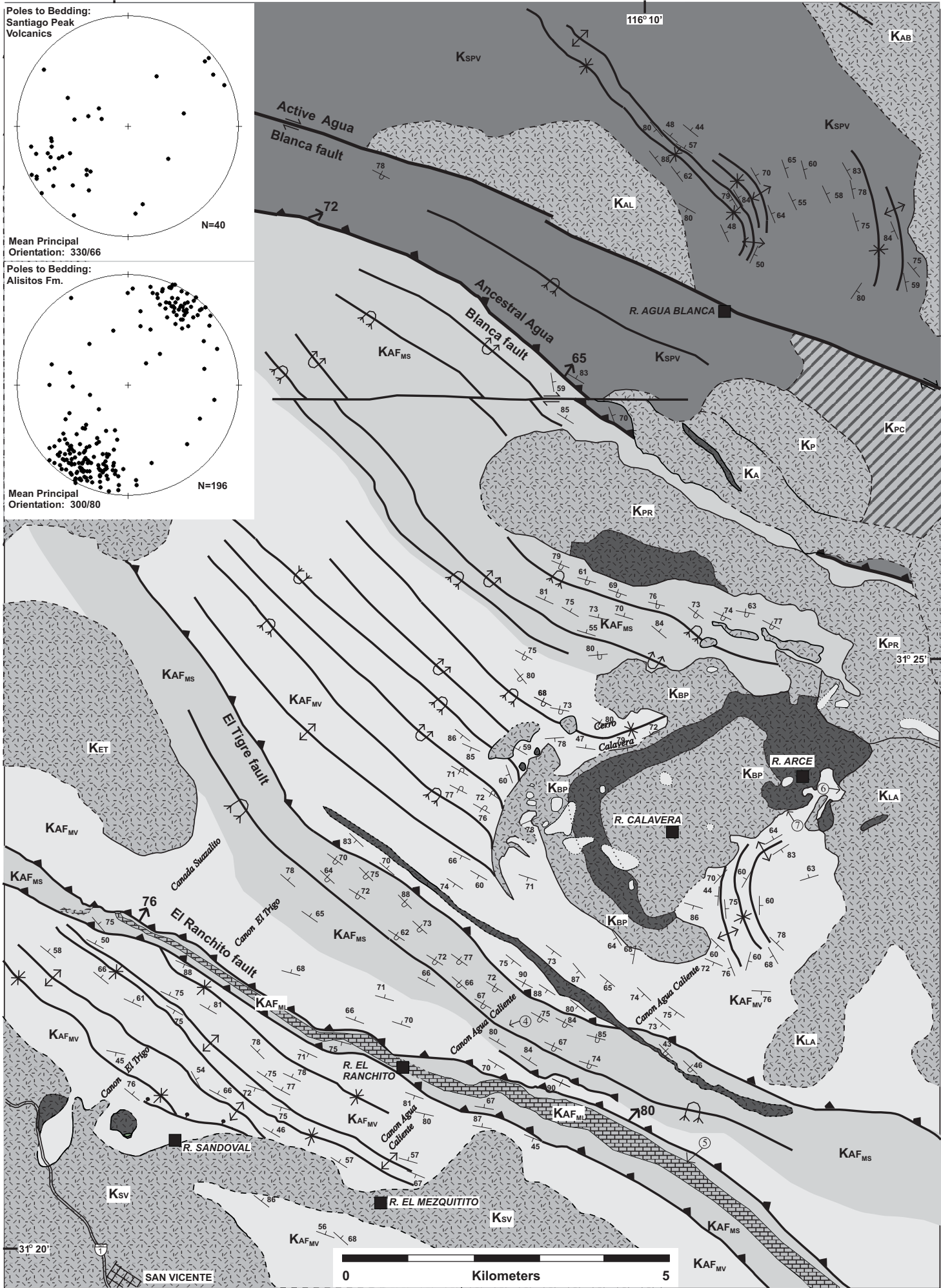
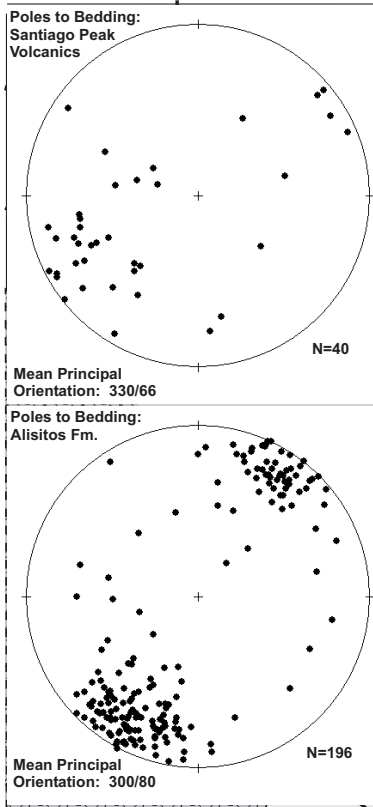


Fig. 3a



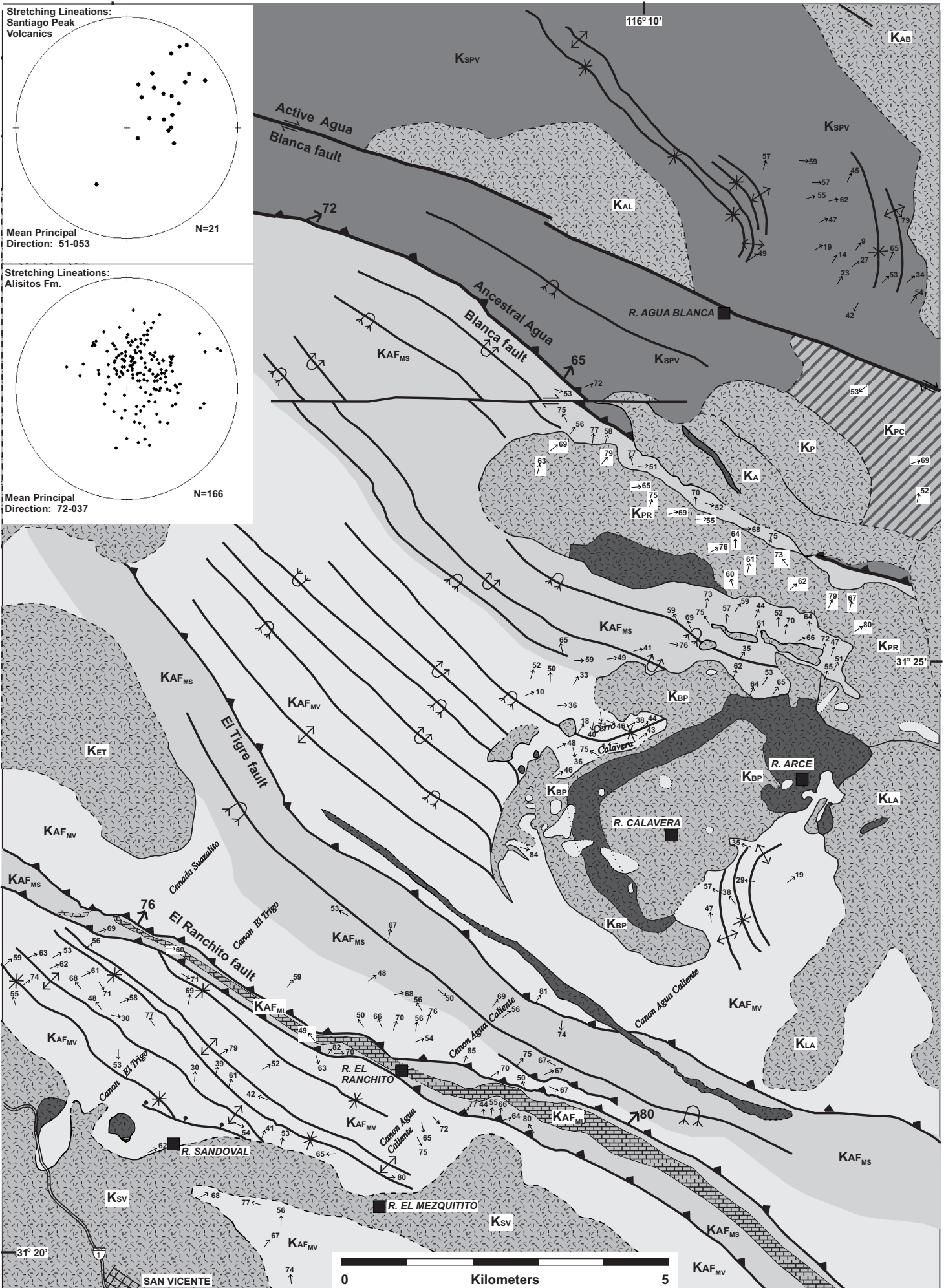
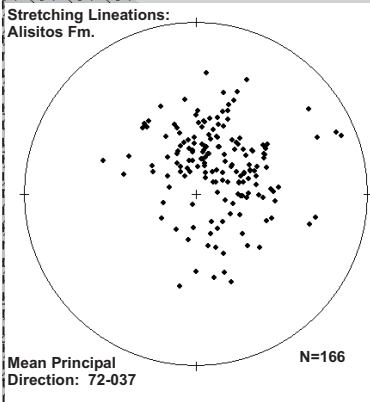
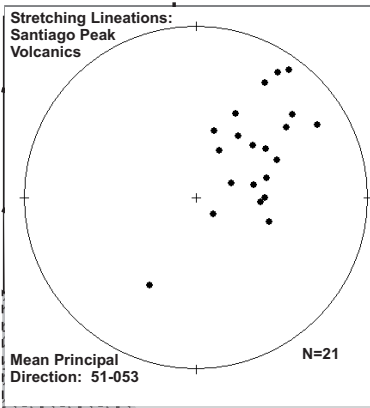


Fig. 3c

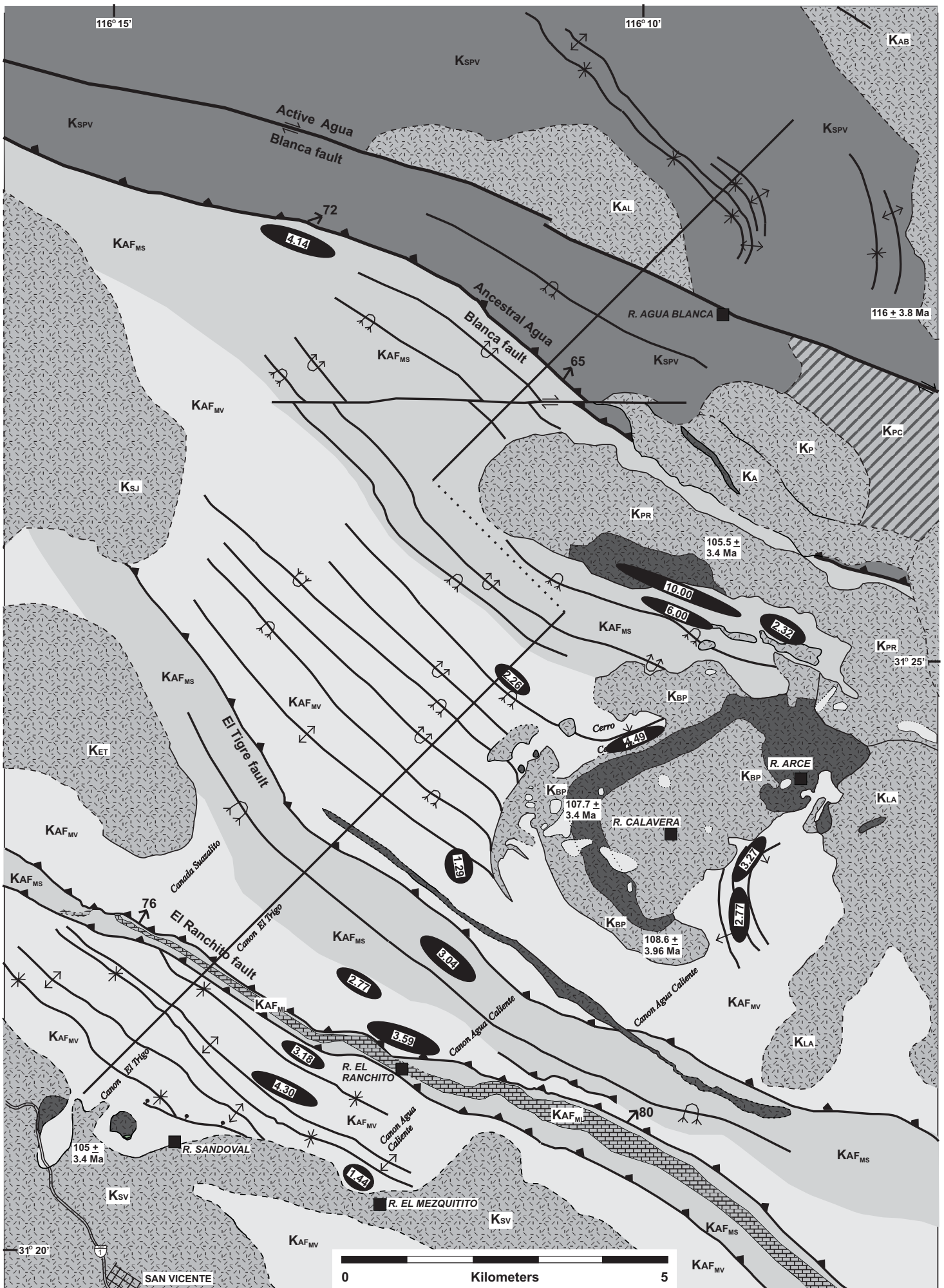


Fig. 3d

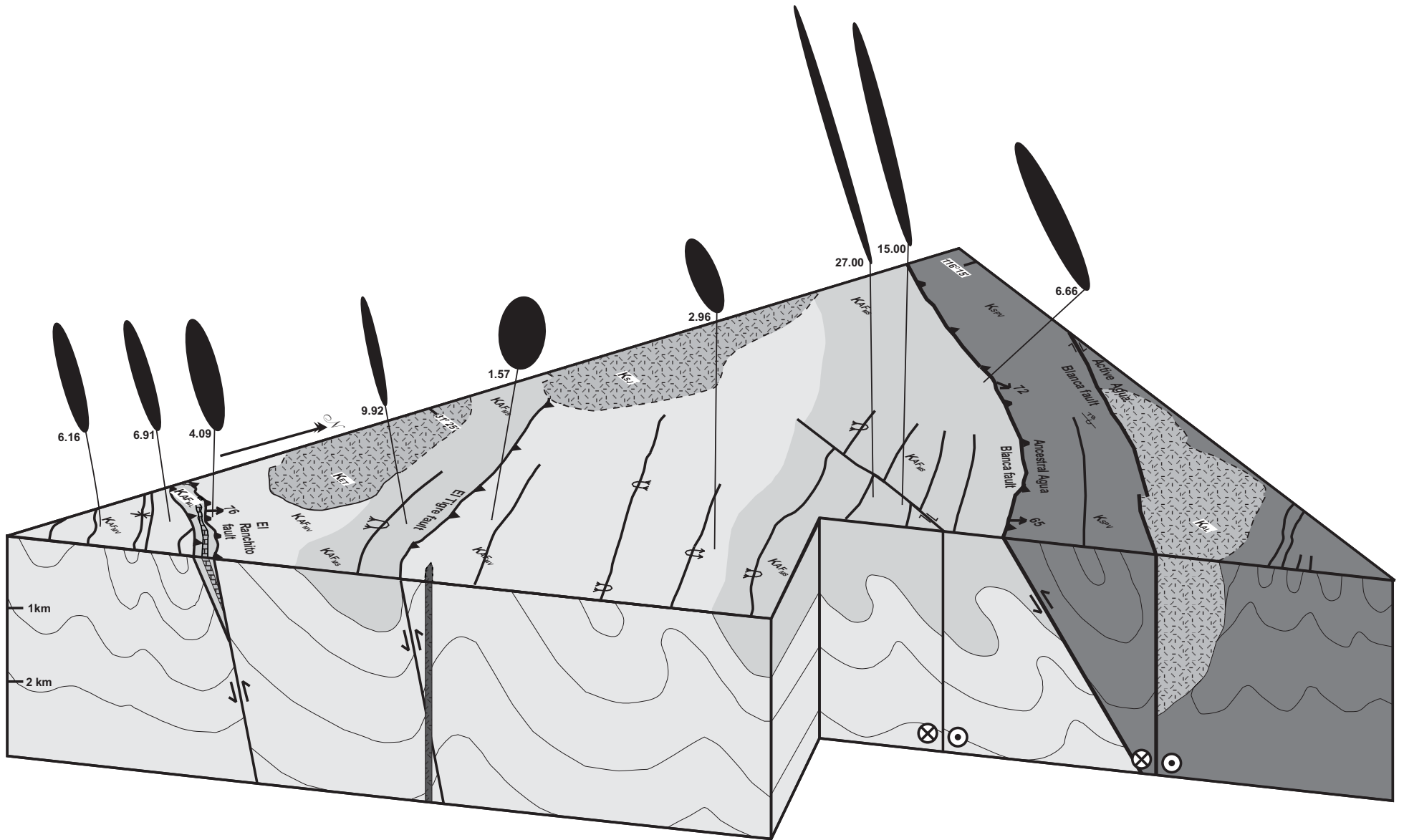


Fig. 3e

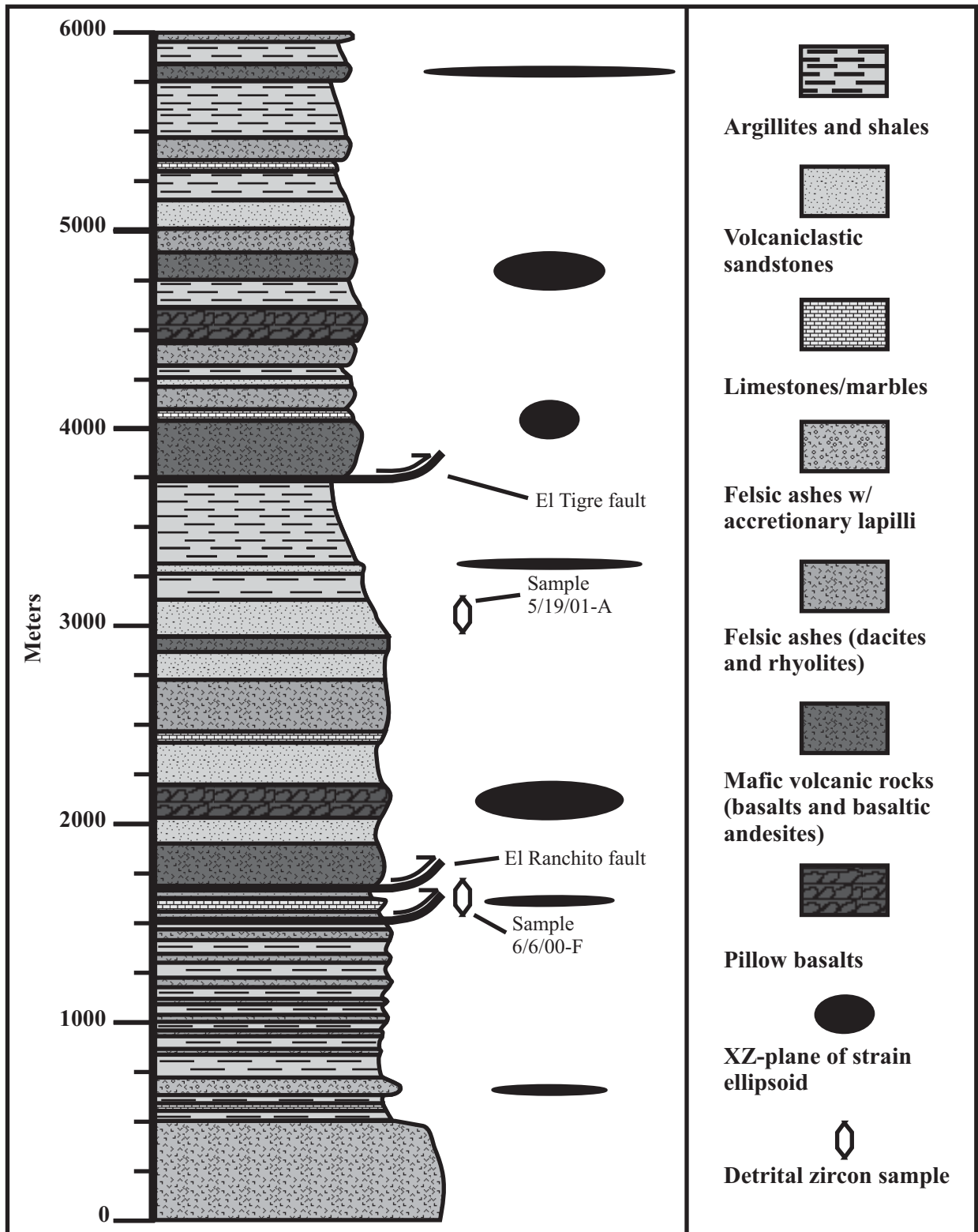


Figure 4



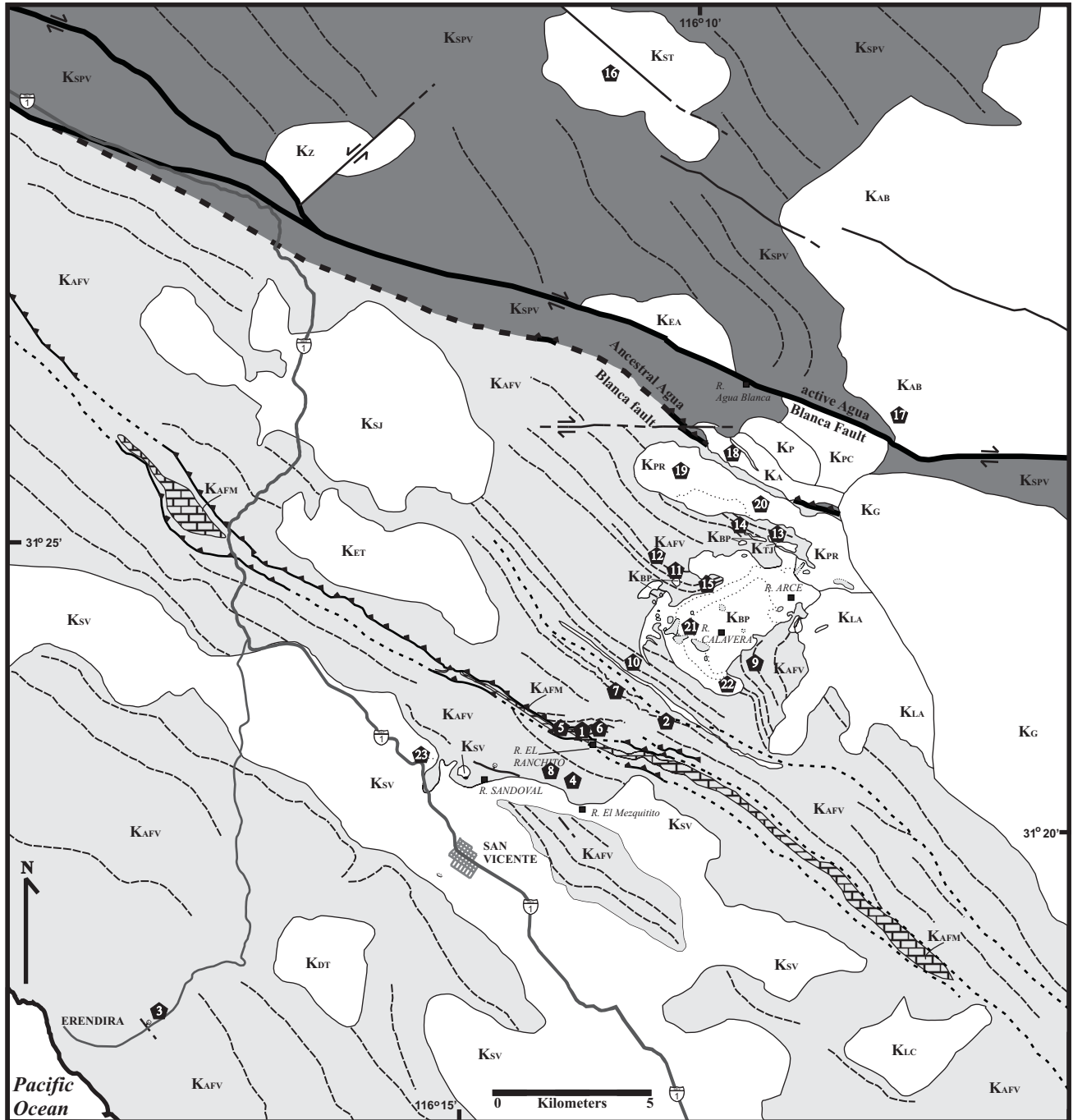
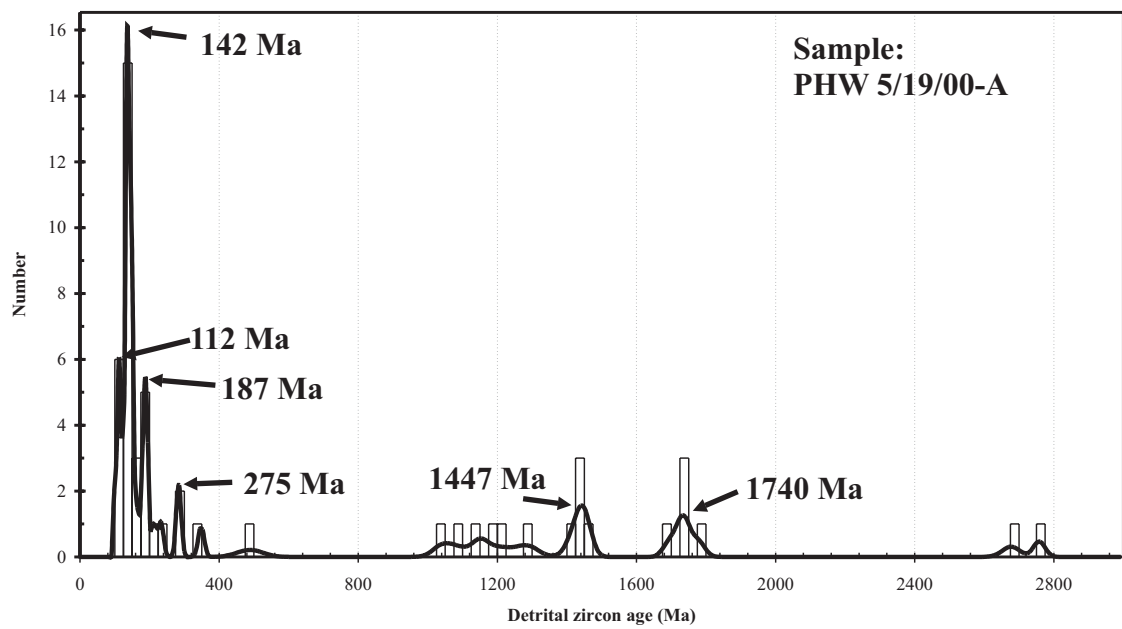
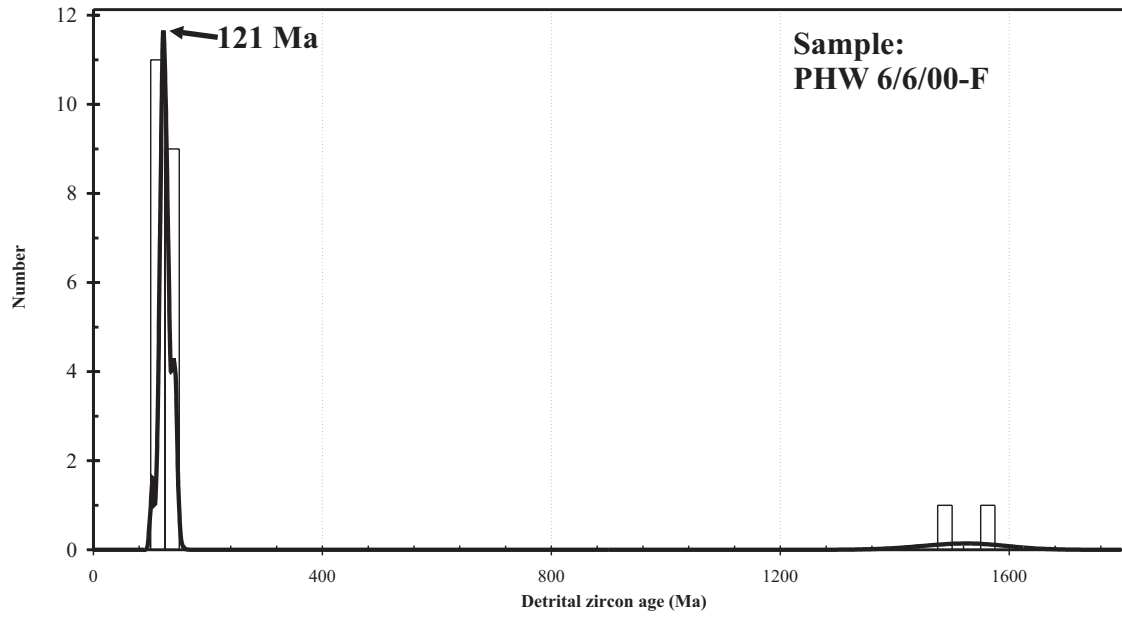


Figure 5.

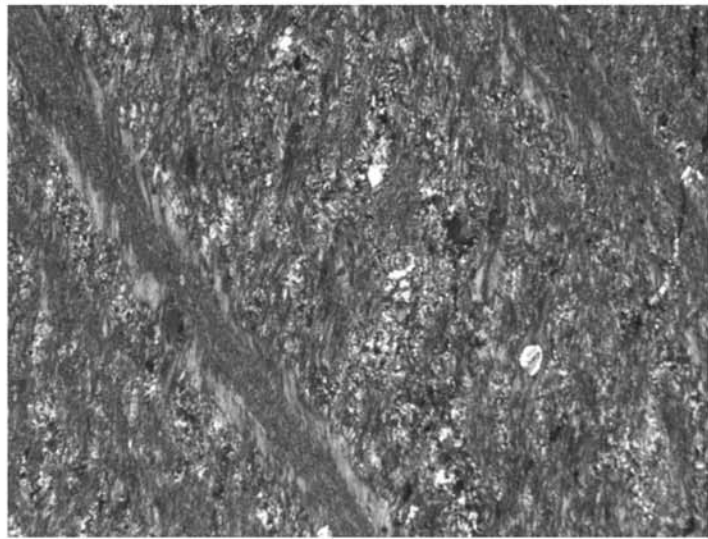


**Figure 6**

**a.**



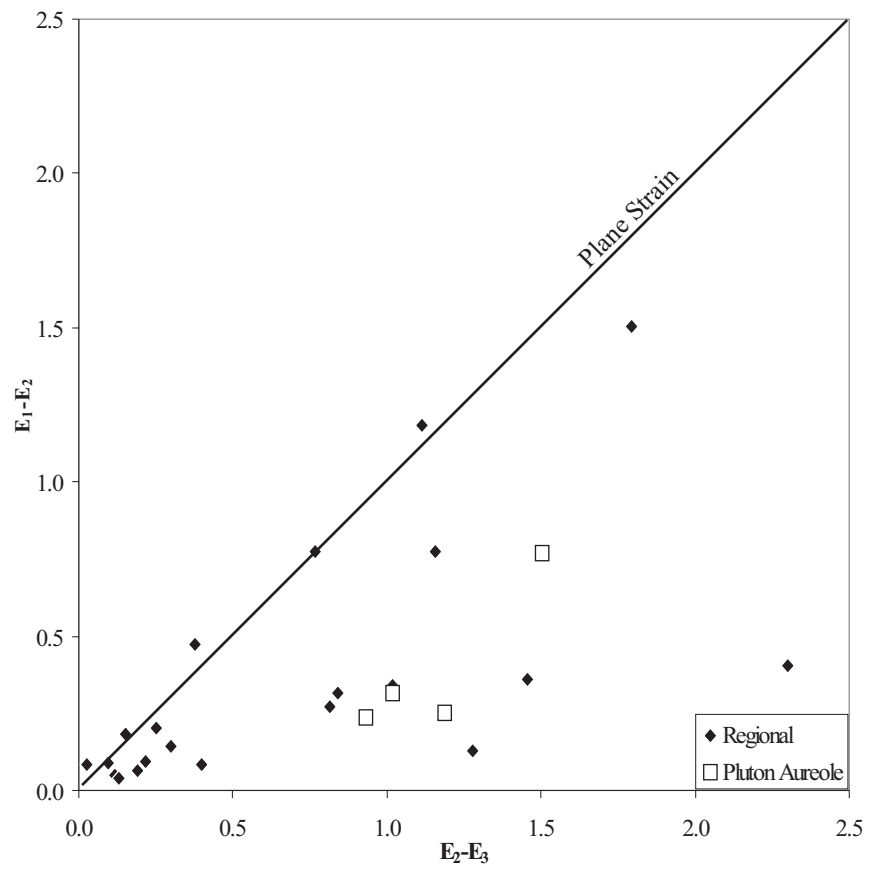
**b.**



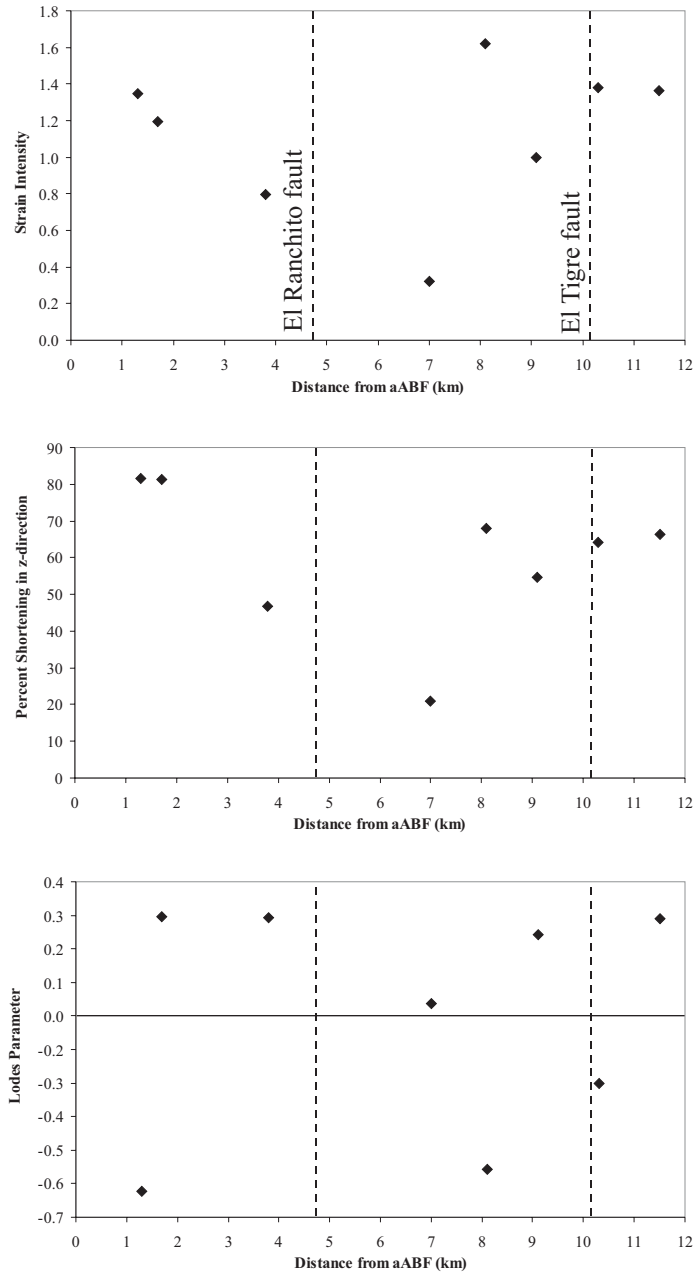
**c.**



Figure 7.



**Figure 8**



**Figure 9**

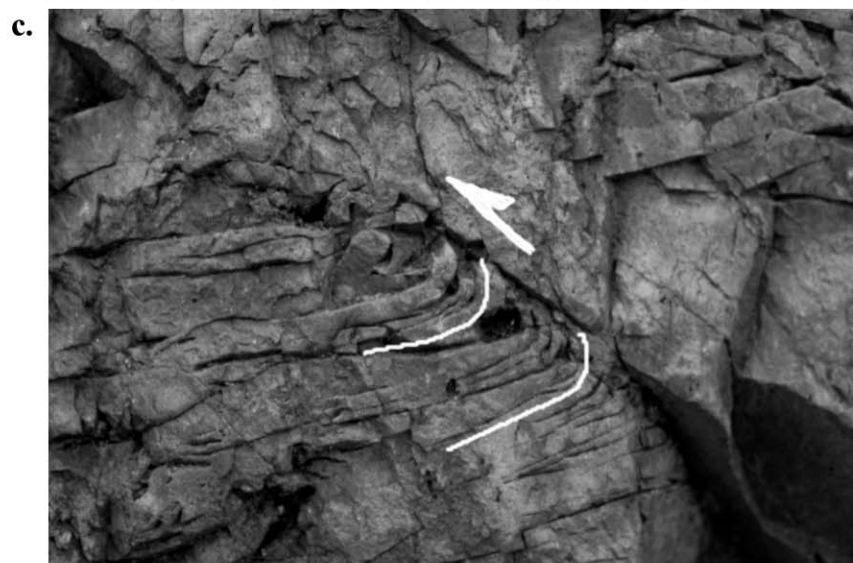
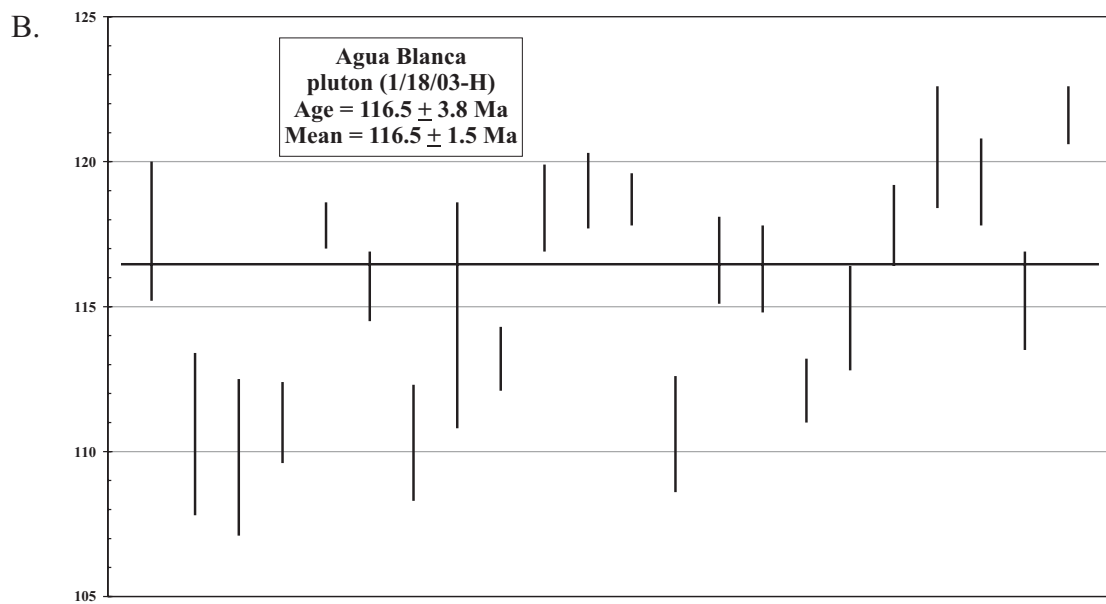
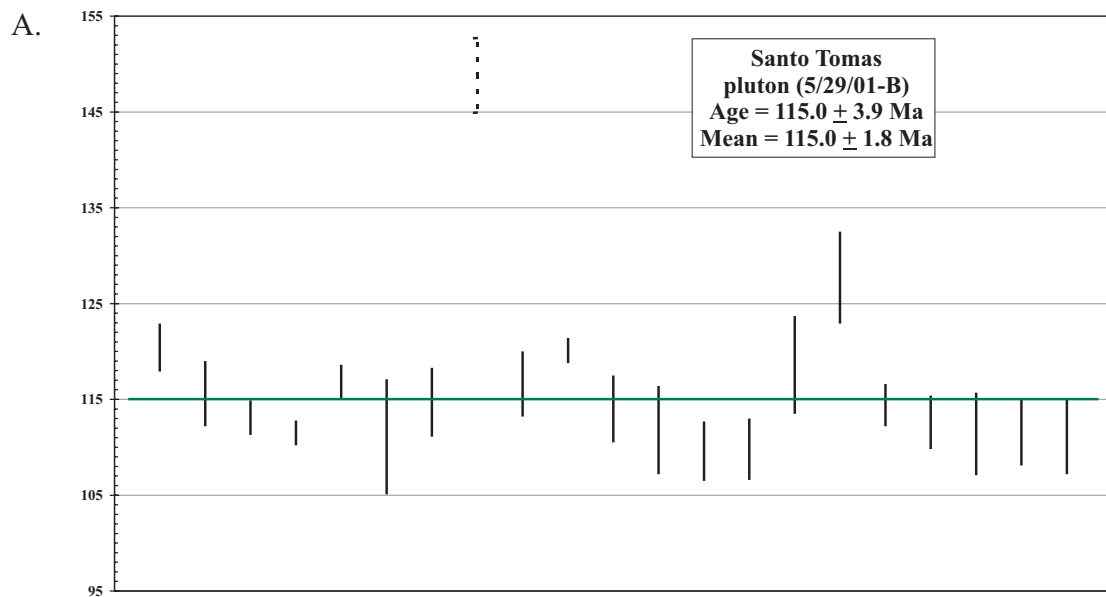


Figure 10.



**Figure 11**

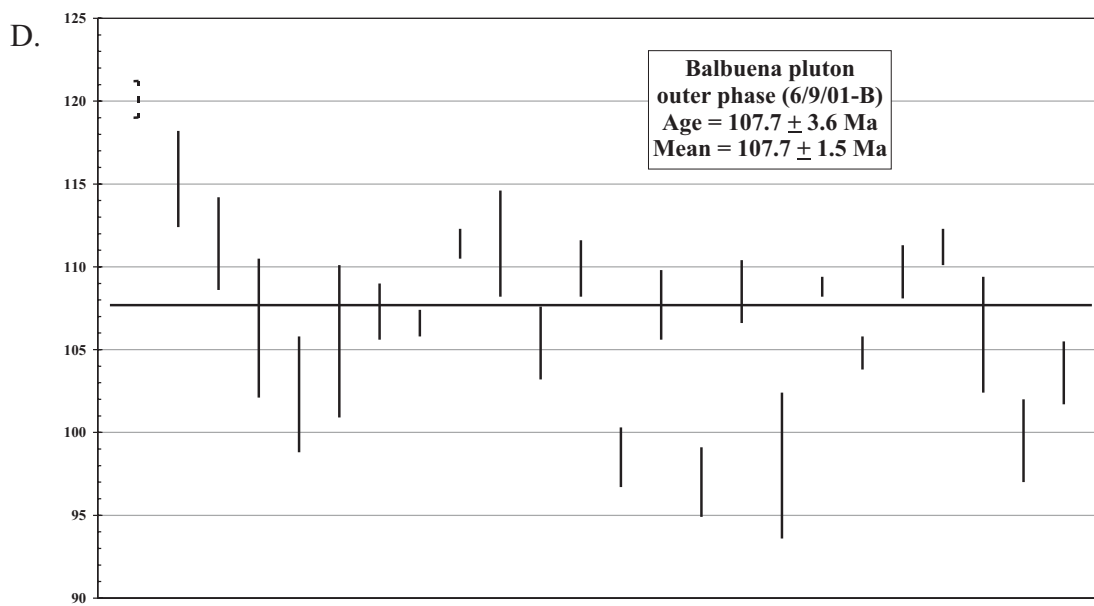
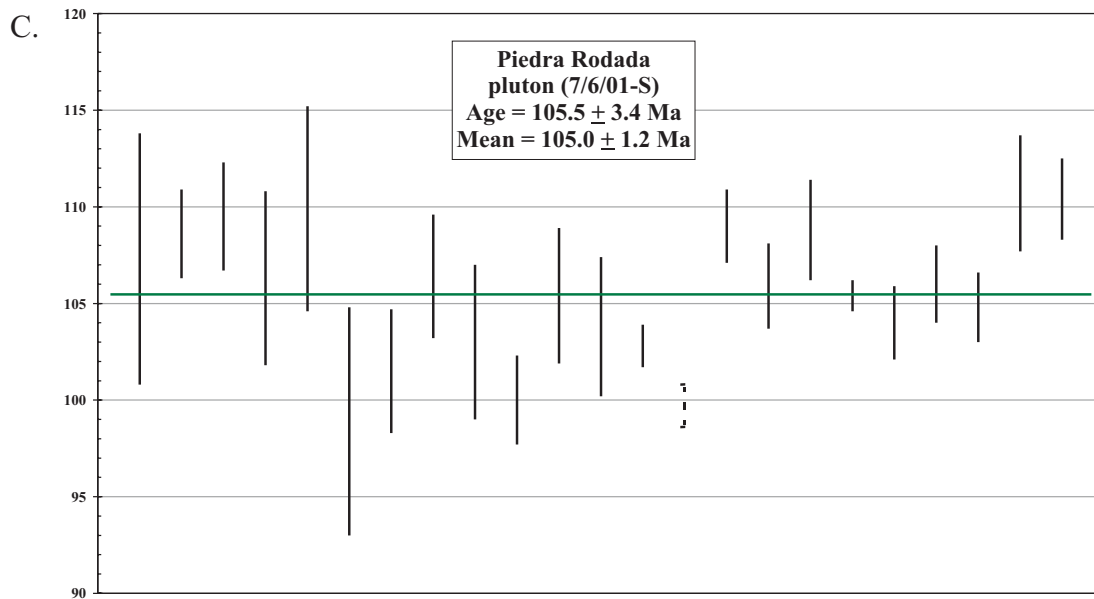


Fig. 11cont'



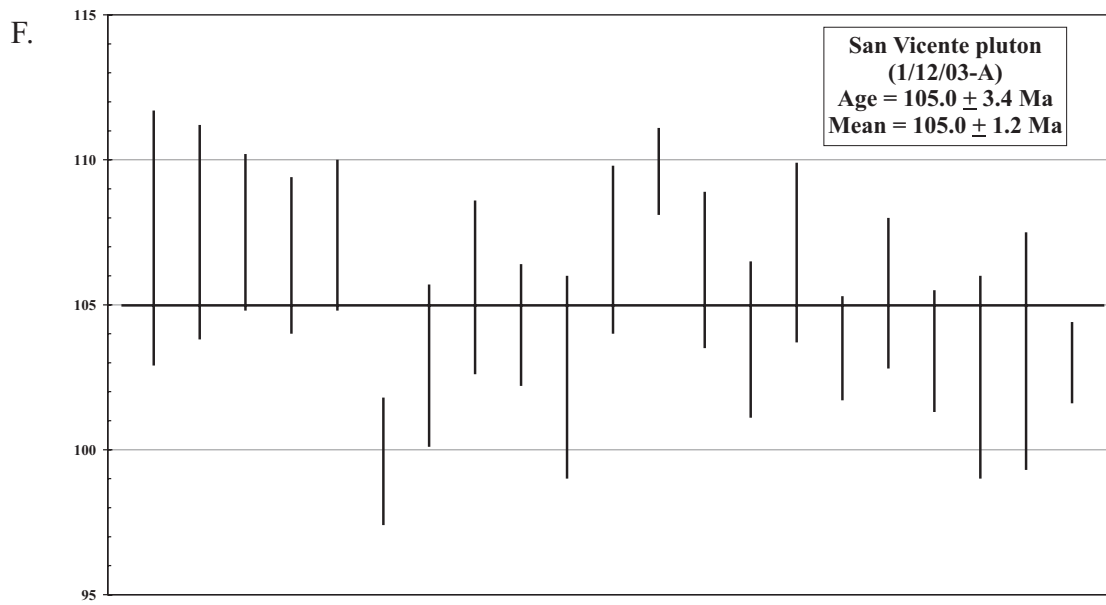
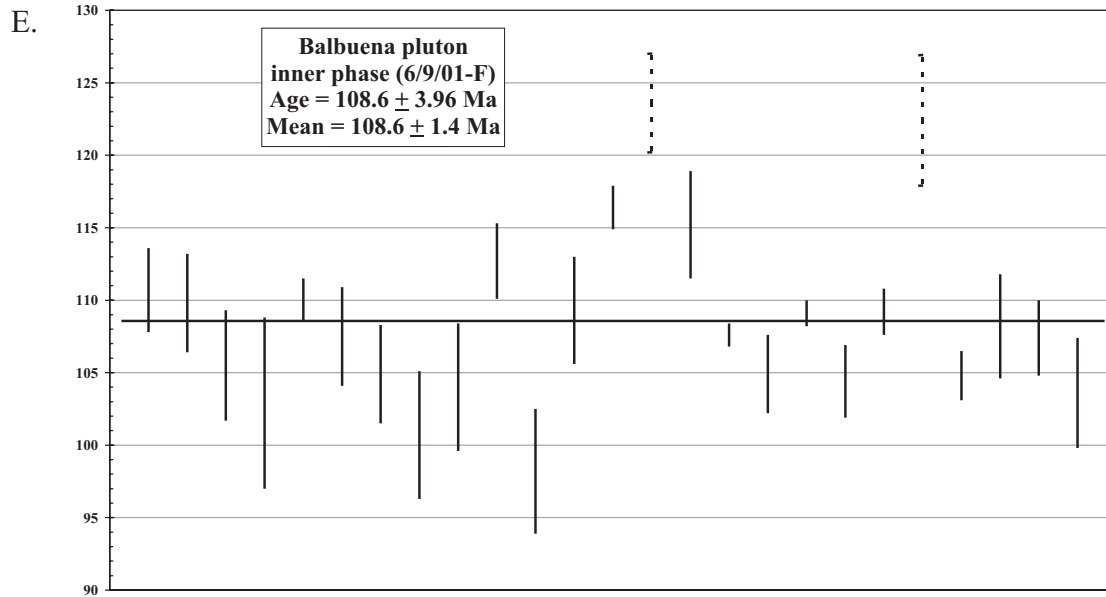


Fig. 11cont'

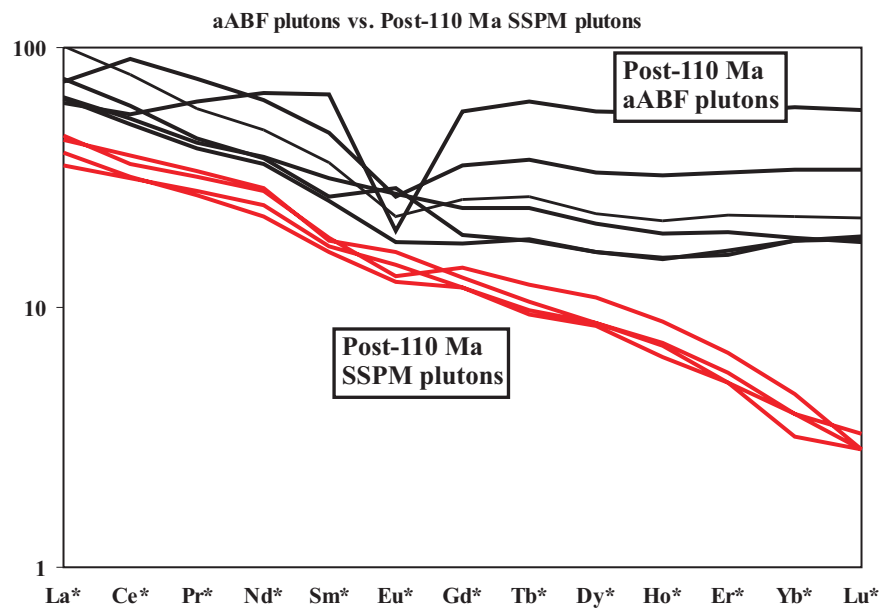


Figure 12.

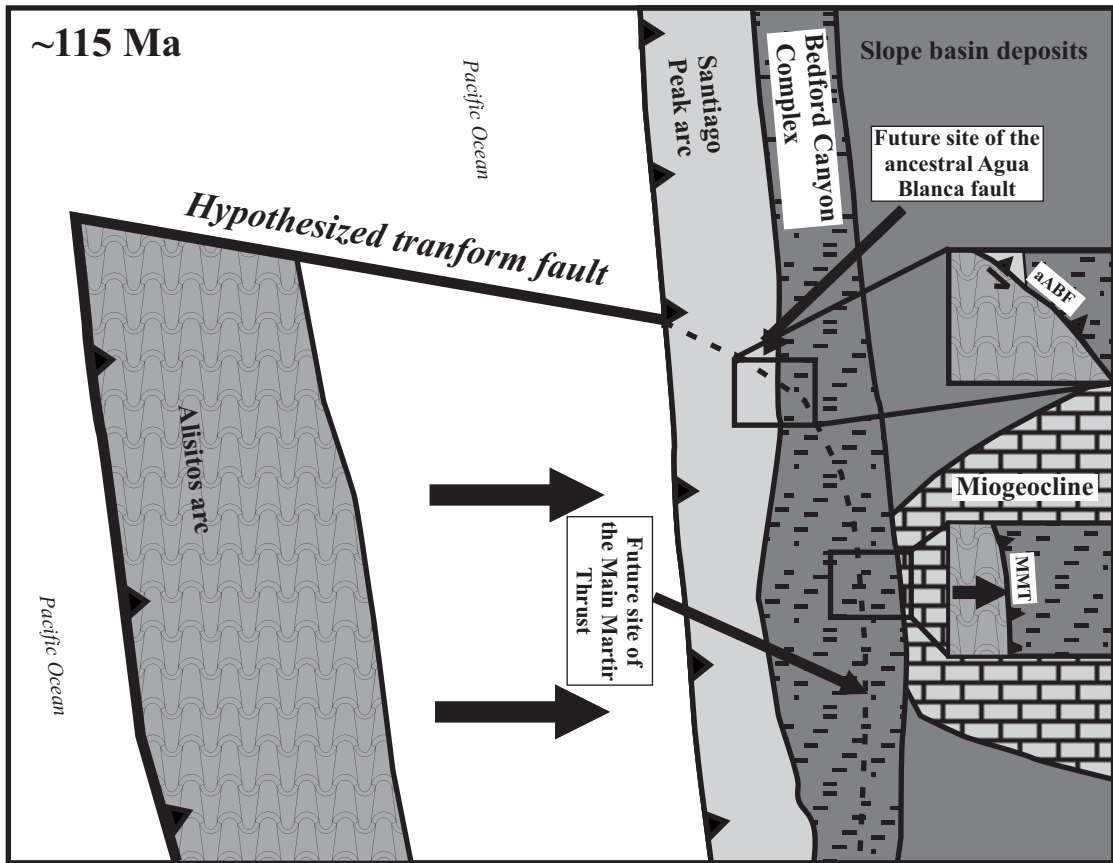


Figure 13.